JGR Solid Earth

RESEARCH ARTICLE
10.1029/2024JB029385

Topography Response to Horizontal Slab Tearing and Oblique Continental Collision: Insights From 3D Thermomechanical Modeling

Giridas Maiti[1], Alexander Koptev[2], Paul Baville[1], Taras Gerya[3], Silvia Crosetto[2], and Nevena Andrić-Tomašević[1]

[1]Institute of Applied Geosciences, Karlsruhe Institute of Technology, Karlsruhe, Germany, [2]GFZ German Research Centre for Geosciences, Potsdam, Germany, [3]Institute of Geophysics, ETH Zurich, Zurich, Switzerland

Key Points:

- We explored numerically in 3D the topography response to horizontal slab tearing during retreating oblique continental collision
- Horizontal slab tearing can initiate before collision due to the transition from oceanic to continental subduction below fore- and back-arc domain
- Surface uplift associated with slab tearing is more pronounced and spreads laterally much faster than in the subsequent collision phase

Supporting Information:

Supporting Information may be found in the online version of this article.

Correspondence to:

G. Maiti,
giridas.maiti@kit.edu

Citation:

Maiti, G., Koptev, A., Baville, P., Gerya, T., Crosetto, S., & Andrić-Tomašević, N. (2024). Topography response to horizontal slab tearing and oblique continental collision: Insights from 3D thermomechanical modeling. *Journal of Geophysical Research: Solid Earth*, *129*, e2024JB029385. https://doi.org/10.1029/2024JB029385

Received 23 APR 2024
Accepted 26 SEP 2024

Author Contributions:

Conceptualization: Giridas Maiti, Alexander Koptev, Taras Gerya, Nevena Andrić-Tomašević
Data curation: Giridas Maiti
Formal analysis: Giridas Maiti, Alexander Koptev, Paul Baville, Silvia Crosetto, Nevena Andrić-Tomašević
Funding acquisition: Nevena Andrić-Tomašević
Investigation: Giridas Maiti
Methodology: Giridas Maiti, Alexander Koptev, Paul Baville, Taras Gerya

Abstract

The horizontal propagation of slab detachment (slab tearing) is known to control lateral migration of the mountain uplift along the collisional belt. However, along-strike differential collision due to an oblique passive margin geometry can make the topography response more complex. In this study, we employ 3D thermomechanical modeling to distinguish between the lateral migration of the mountain topography driven by slab tearing and oblique continental collision itself. In our models, slab breakoff is triggered by the transition from oceanic to continental subduction, occurring earlier on one side of the passive margin than on the other due to the initial oblique configuration. However, once slab breakoff has begun, it spreads horizontally in the form of tearing at high velocity (~38–118 cm yr^{-1}), and associated topographic uplift also propagates with the same velocity. In contrast, the along-strike migration of subsequent continental collision and related topographic uplift propagation is typically much slower (~2–34 cm yr^{-1}). Similarly, the vertical magnitude of surface uplift caused by slab tearing is higher (up to 10 mm yr^{-1}) than the following collision phase (<4 mm yr^{-1}). The parametric analysis reveals that slab tearing velocity and the associated horizontal propagation of mountain uplift depends on obliquity angle and slab age, whereas the migration of collision-induced topographic growth is controlled by the convergence velocity and obliquity angle. Finally, we show that presence of microcontinental block detached from the passive margin leads to spatial and temporal transition from horizontal to vertical slab tearing and more intense syn-collisional mountain building.

Plain Language Summary

Continental collision begins after the complete subduction of the oceanic domain, initially located between the colliding continents. As the oceanic slab has negative buoyancy, it detaches from the positively buoyant continental plate shortly after the start of continental collision. Slab detachment leads to a rapid uplift of the surface topography and usually moves sideways, a process known as slab tearing. Slab tearing in turn results in a lateral propagation of the topographic uplift along the continental margin. However, if the colliding plate margins are initially at an angle to each other, an oblique continental collision occurs, which can also lead to along-strike migration of the mountain uplift. To differentiate between the topography response to slab tearing and oblique continental collision, we have carried out 3D numerical modeling. Our parametric analysis reveals that the rate of slab tearing and the associated horizontal propagation of mountain uplift primarily depend on the angle of collisional obliquity and the age of the subducting oceanic slab, whereas the velocity of plate convergence controls the migration of collision-induced topographic growth. Our findings also indicate that the surface uplift associated with slab tearing is more pronounced and spreads laterally much faster than during following oblique continental collision.

1. Introduction

The formation of mountain belts in continental collision zones results from the closure of an oceanic domain, which is accompanied by crustal thickening and surface uplift. The collisional mountain belts are mechanically coupled to the adjacent foreland basins (Stockmal et al., 1987), where sediments coming from the mountain belts are deposited. Consequently, the sedimentary archives of the foreland basin record most of the tectonic history of mountain building. However, the evolution of mountain belts and associated sedimentary basins are observed to be variable in an orogen-parallel direction (Angrand et al., 2018; Galewsky & Silver, 1997; Gül et al., 2015; Kuhlemann & Kempf, 2002; Lash, 1998; Nagel et al., 2013). Slab tearing, a lithospheric-scale process, is commonly used to explain such along-strike variations in different collisional settings. These include, for example, migration of the surface uplift of the intramountain basins within the Betics and Rif (Boonma

Project administration: Nevena Andrić-Tomašević
Resources: Nevena Andrić-Tomašević
Software: Giridas Maiti, Alexander Koptev, Taras Gerya
Supervision: Taras Gerya, Nevena Andrić-Tomašević
Validation: Giridas Maiti, Alexander Koptev, Taras Gerya, Silvia Crosetto, Nevena Andrić-Tomašević
Visualization: Giridas Maiti, Paul Baville
Writing – original draft: Giridas Maiti
Writing – review & editing: Giridas Maiti, Alexander Koptev, Taras Gerya, Silvia Crosetto, Nevena Andrić-Tomašević

et al., 2023), foreland basin depocenter migration along the Alps-Carpathians fold and thrust belt (Meulenkamp et al., 1996), and lateral shifts of Apenninic foredeep depocenters (van der Meulen et al., 1998). In addition, irregularities in the architecture of the original boundary between the continental and oceanic domains on the subducting plate (e.g., an obliquity of passive margin or subduction zone) are known to control along-strike diachrony in the resulting continental collision (e.g., Darin & Umhoefer, 2022; Nagel et al., 2013). This is also reflected in associated sedimentary processes, as exemplified by the Aquitane, Kahramanmaras, Appalachian, and Western foreland basins (Angrand et al., 2018; Gül et al., 2015; Lash, 1998; Nagel et al., 2013). This implies that both slab tearing and differential collision have an influence on the along-strike variability in the evolution of the mountain belt and adjacent basins. However, it is difficult to decipher the relative contribution of these two processes based on geologic observations alone. In this study, using 3D thermomechanical numerical modeling we investigate the role of initial obliquity of the passive margin in subsequent slab tearing and continental collision to quantify the effects of these processes on the along-strike topographic development.

2. Background

Slab breakoff (detachment) in the literature is described as a buoyancy-driven geodynamic process that usually occurs during an early continental collision, when the heavy oceanic plate detaches from the light continental lithosphere after cessation of active subduction (Davies & Von Blanckenburg, 1995; Wortel & Spakman, 1992, 2000). This is not to be confused with the removal of mantle lithosphere through so-called "dripping" and "delamination," which also involve the separation and foundering of negatively buoyant material, but which are fundamentally different from the slab breakoff phenomena. In particular, the term "delamination" refers to the peeling away of the mantle lithosphere (without any internal deformation) along a decollement layer, that often corresponds to the lowermost crust (Göğüş & Pysklywec, 2008), whereas "dripping" involves the removal of cold, dense mantle lithosphere by viscous Rayleigh–Taylor instability (Pysklywec et al., 2000), resulting in substantial internal deformation, that proceeds on longer time scales but remains axisymmetric and exhibits little to no lateral migration (Göğüş & Pysklywec, 2008).

Previous studies have linked slab breakoff to a variety of geologic observations at the surface, including magmatic flare-ups (Zhu et al., 2015), rapid topographic uplift (Huang et al., 2010), increasing sediment supply (Sinclair, 1997), rapid exhumation of metamorphic rocks (O'Brien, 2001; Sizova et al., 2019), and others as summarized in Garzanti et al. (2018). Using the 3D seismic velocity structure of the upper mantle in the Mediterranean region, Wortel and Spakman (1992, 2000) first proposed that the rupture of a subducting plate, once initiated on one of its segments, can migrate laterally, a process now known as slab tearing (Menant et al., 2016). The first 3D numerical models, performed more than a decade later (Burkett & Billen, 2010; van Hunen & Allen, 2011), showed that in the case of a laterally symmetric and homogeneous subducting lithosphere, the onset of slab breakoff occurs almost simultaneously along the entire length of the plate. However, when heterogeneity is introduced (in the form of continental blocks or mid-ocean ridge segments), the slab rupture begins in the rheologically weakest area and then propagates laterally (Burkett & Billen, 2010; van Hunen & Allen, 2011). It is commonly accepted that breakoff is a rapid process, taking only a few Myr from the initial necking of the slab to its complete detachment (Duretz et al., 2011; Gerya et al., 2004). Importantly, the horizontal propagation of slab breakoff (slab tearing), which has so far been determined in numerical experiments, is also very fast, reaching a rate of ∼80 cm yr^{-1} (Burkett & Billen, 2010; van Hunen & Allen, 2011) and even >100 cm yr^{-1} (Andrić-Tomašević et al., 2023).

In most previous 3D modeling studies, an initial passive margin either extends parallel to the subduction trench (Burkett & Billen, 2010; van Hunen & Allen, 2011) or there is an abrupt "continental corner" to reproduce a sharp transition between simultaneous oceanic subduction and continental collision (Duretz et al., 2014; Li et al., 2013; Menant et al., 2016; Sternai et al., 2014). However, collision can also occur along an oblique passive margin, as shown by paleogeographic and paleotectonic reconstructions in the Taiwan arc (Barrier & Angelier, 1986; Chemenda et al., 2001), in the Bismark arc of Papua New Guinea (Galewsky & Silver, 1997), in the Alps (Eskens et al., 2024; Handy et al., 2010), in the Betic Cordillera (Boonma et al., 2023; Vergés & Fernàndez, 2012), and the Zagros (Darin & Umhoefer, 2022; Tesauro et al., 2024). Importantly, such original obliquity not only leads to a gradual change from ocean-continent subduction to continent-continent collision, but also affects the slab breakoff and tearing together with a response of surface topography and sedimentary basins, as recently demonstrated on the example of the Gibraltar Arc region (Boonma et al., 2023). Depending on the relative position of the actively moving plate (subducting or overriding), the continental collision can occur in either

advancing (e.g., Duretz et al., 2014; Li et al., 2013; Menant et al., 2016; Sternai et al., 2014; van Hunen & Allen, 2011) or retreating (Boonma et al., 2023) manner, which may affect the dynamics of slab breakoff and tearing and the associated topography reaction. The retreating collision is observed in nature (e.g., Faccenna et al., 2014) but rarely modeled (Boonma et al., 2023), so it requires further numerical investigation.

According to observations in various sedimentary basins, mostly forelands formed in front of the growing orogen, such as along the Alpine-Carpathian chain (Meulenkamp et al., 1996) and the Apennines (van der Meulen et al., 1998), estimated rates of slab tearing are in between ∼5 and <45 cm yr^{-1}. However, as mentioned above, slab tearing in 3D numerical models is a much faster process, with rates ranging from ∼35 to 150 cm yr^{-1} leading to a rapid completion (typically within ∼1–2 Myr) of full slab detachment along its entire modeled extent (Andrić-Tomašević et al., 2023; Boonma et al., 2023; Burkett & Billen, 2010; van Hunen & Allen, 2011). This serious discrepancy between the observed and modeled rates of tear propagation calls into question the validity of the hypothesis that slab tearing is a main driver for the shallowing of sedimentary basins due to tectonic uplift and topographic growth that progressively develop along the collisional belt.

Since the process of continent-continent collision itself leads to crustal thickening and topographic uplift, it is important to consider obliquity or other irregularities at the original continental margins as a factor in the diachroneity of the resulting continental collision (Darin & Umhoefer, 2022), which may also lead to along-strike migration of topographic uplift and basin depocenters. However, as slab tearing and collision are coupled processes, estimating their relative contributions to the evolution of topography and sedimentary basins is uncertain. Using a 3D thermomechanical modeling approach, this study aims to investigate how the transition from retreating subduction to oblique continental collision controls both slab tearing and collision-induced topographic changes. By distinguishing between topography response to slab tearing and to retreating collision itself, we address the question of what are the main factors influencing the development of differential surface uplift along the orogen and the potential impact on the associated foreland basin.

3. Numerical Methods

We have investigated the processes of slab tearing and oblique retreating continental collision using the 3D thermomechanical code I3ELVIS (Gerya, 2019; Gerya & Yuen, 2007), which is based on finite-difference and marker-in-cell methods (Gerya & Yuen, 2003). The code solves the momentum, continuity, and energy equations on the fixed Eulerian grid and transports the physical properties by Lagrangian markers using the velocity field. The code also accounts for the major phase transitions in the Earth's mantle and internal heat sources arising from adiabatic, radiogenic, and frictional heating. Partial melting and melt extraction processes are neglected for the sake of simplicity. A more detailed description of the code, including the governing equations and the adopted rheological model, is provided Text S1 in the Supporting Information S1.

3.1. Model Setup

The 3D model area has a size of 2,000 km (x) × 1,200 km (y) in the horizontal directions and 780 km in the vertical direction (z). The model consists of 433 × 261 × 261 nodes with a spatial grid resolution of ∼4.6 × 4.6 × 3.0 km in x-, y- (horizontal) and z- (vertical) direction, respectively. This results in more than 20 million elements with six Lagrange markers per element which requires a high computation time. The lithospheric domain consists of the continental plate on the left side of the model and the oceanic plate on the right side, which also includes a continental block with horizontal dimensions of 500 × 800 km (Figure 1a). Within the lithosphere of this continental block (in a vertical plane at x = 1,800 km for a depth range of z = 21–147 km), we impose a constant horizontal velocity (0–4.5 cm yr^{-1}) that mimics the plate driving forces arising from ridge push (Artyushkov, 1973; Koptev & Ershov, 2010) and/or basal drag (Bird et al., 2008) to initiate the retreating ocean-continent subduction. The initiation of subduction (Andrić et al., 2018; Koptev et al., 2022; Stern & Gerya, 2018) along the left boundary of the right continent is enabled by prescribing lithospheric-scale zone of weakness, dipping at an angle of ∼30° to the horizontal plane (Figure 1b). The horizontal width of this inclined weak zone varies between 10 km at the surface and 5 km at a depth of 110 km (Figure 1b). Additionally, two lithospheric-scale vertical weak zones are prescribed at the front and back edge of the moving continental plate in order to decouple it from the surrounding oceanic plate and allow its movement toward the left continental plate. These vertical weak zones have a constant thickness of 10 km and are only prescribed to facilitate the initial stage of continental plate movement (e.g., Balázs et al., 2021; Boonma et al., 2023), without having any influence on the

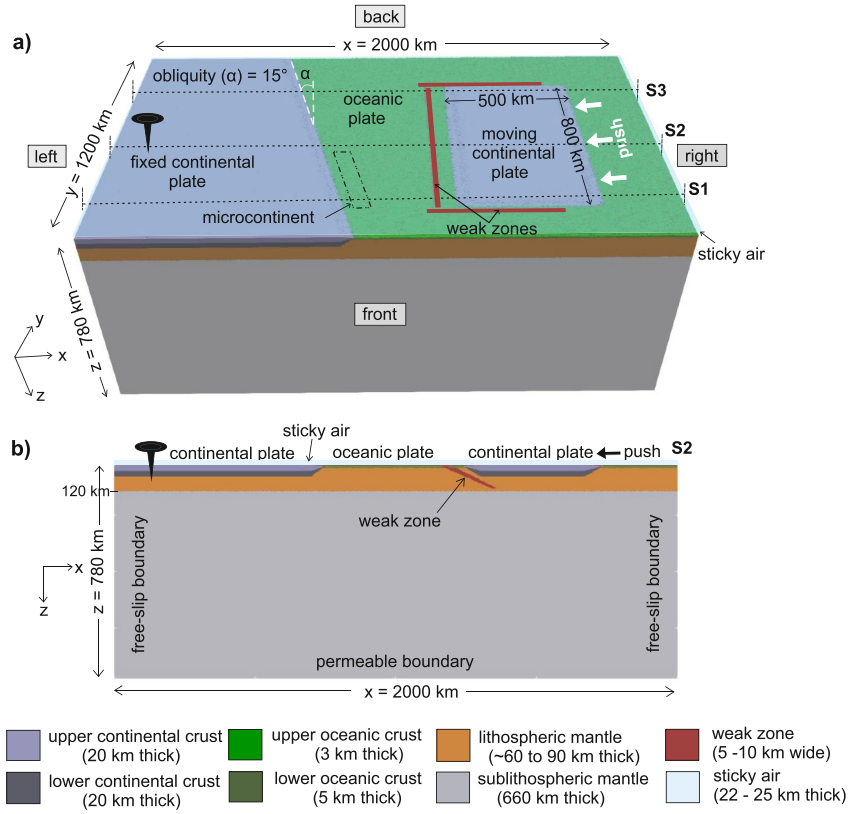

Figure 1. Initial model setup. (a) 3D view of the compositional field. Note the obliquity of the passive continental plate margin indicated for the reference case ($\alpha = 15°$) but varying in the different experiments, and the dashed rectangle represents a microcontinent, absent in the reference model but implemented in a limited set of models (Table 1). The white bold arrow marks the direction and location of a prescribed push on the right side of the moving continental plate. The black dotted lines show the locations of the vertical profiles S1, S2 and S3 shown in subsequent figures (Figures 2, 3, 5, 7, 8, and 9). (b) Displays the vertical profile along S2. Note the weak zone that dips beneath the right continent and allows the onset of oceanic subduction, the direction of plate convergence, and the kinematic boundary conditions at the vertical and lower boundaries.

later phases of model development. The left continent always remains stationary and its passive margin is oblique with respect to the orientation of the active margin (subduction zone) between the oceanic lithosphere and the continent in the right part of the model. To understand how oblique retreating plate convergence and differential continental collision affect slab tearing and along-strike evolution of mountain topography, we systematically varied the initial obliquity angle of the passive margin (see Section 3.3). Furthermore, in several experiments we also included a microcontinental block close to the original passive margin to account for additional complications and structural heterogeneities observed in natural collisional systems (Angrand et al., 2018; Darin & Umhoefer, 2022; Gül et al., 2015; Lash, 1998; Manatschal & Müntener, 2009; Mohn et al., 2014).

Following previous modeling studies (Andrić-Tomašević et al., 2023; Boonma et al., 2023), we assume for both the right and left continental plates that the 40-km thick continental crust is evenly divided into an upper felsic (20 km) and a lower mafic (20 km) crust (Table S1 in Supporting Information S1), while their ductile rheologies are defined by flow laws for wet quartzite and plagioclase, respectively (Table S2 in Supporting Information S1). The 8-km thick oceanic crust consists of upper basaltic (3 km) and lower gabbroic (5 km) layers (Tables S1 and S2 in Supporting Information S1). The lithospheric and sublithospheric mantle is governed by a dry olivine rheology (Hirth & Kohlstedt, 2004), while the lower effective viscosity of the weak zones around the right continental block is implemented by extremely low values of brittle strength (Table S2 in Supporting Information S1). For the ultramafic lithospheric and sublithospheric mantle, we assigned identical rheological properties (assigned using a Christmas-tree-like criterion; Ranalli, 1995) and density (computed as a function of temperature and pressure from the thermodynamic model Perple_X; Connolly, 2005), so that the base of the lithosphere is defined by the

depth of the 1,300°C isotherm (Artemieva, 2006; Koptev & Ershov, 2011). In contrast, the felsic upper continental crust differs from the mafic layers of the lower continental and upper and lower oceanic crust in terms of both rheology and reference densities. All values for densities and thermal parameters (Bittner & Schmeling, 1995; Clauser & Huenges, 1995; Turcotte & Schubert, 2002) as well as rheological properties (Burov, 2011; Hirth & Kohlstedt, 2004; Ranalli, 1995) can be found in Tables S1 and S2 in Supporting Information S1. The original thermal structure of the oceanic lithosphere is defined using a half-space cooling approximation (e.g., Turcotte & Schubert, 2002) for plate ages between 20 and 80 Ma (see Section 3.3). For continental plates, a typical steady-state conductive geotherm is assumed (Artemieva, 2006; Koptev & Ershov, 2011) with a lithospheric thermal thickness of ∼100 km and considering the distribution of radiogenic heat production in the lithosphere (Table S1 in Supporting Information S1). The adiabatic gradient in the sublithospheric mantle is initially 0.5 K km^{-1} (Putirka et al., 2007; Sleep, 2003).

In all our models, the oceanic plate is compositionally and thermally homogeneous along the passive margin, without any inherent heterogeneity (Chen et al., 2023), such as geometric irregularities (e.g., mid-ocean or amagmatic ridges) and/or lateral variations in thermal age, rheology, and density.

3.2. Boundary Conditions

Free slip kinematic boundary condition is applied to the left ($x = 0$ km), right ($x = 2{,}000$ km), front ($y = 0$ km), back ($y = 1{,}200$), and upper ($z = 0$) boundaries of the model domain. The free slip condition requires that the two non-orthogonal components of the velocity do not change across the boundary, while the orthogonal component is zero. The lower boundary ($z = 780$ km) is open/permeable, so that rock material can flow into/out of the model domain. In particular, this means that infinite-like external free slip conditions exist at ∼300 km below the base of the model domain, which is at 1,080 km depth (Gerya et al., 2008). Similar to usual free slip, external free slip also satisfies the conditions of zero shear stress and constant normal velocity to ensure mass conservation within the computational domain (Gerya et al., 2008; Li et al., 2013). The elevation of the topography is dynamically calculated as the internal free surface using a buffer layer called "sticky air" ($\eta_{air} = 10^{18}$ Pa s, $\rho_{air} = 1$ kg m^{-3}) (Crameri et al., 2012; Gerya & Yuen, 2003; Schmeling et al., 2008), whose thickness is 22 and 25 km above the continental and oceanic plates, respectively. We implemented a simplified model of erosion/sedimentation in which surface depressions with a depth of 8 km and more below sea level are immediately filled with sediments, while crustal markers at a height of ≥8 km are instantaneously replaced by sticky air (Boonma et al., 2023; Gerya et al., 2008). Considering that these extremely high limits (±8 km) were never reached during the development of the performed experiments, our model of surface processes can be interpreted as the simplest option that excludes any erosion and sedimentation and thus equates the surface uplift/subsidence with the uplift/subsidence of rock (England & Molnar, 1990). A more realistic implementation of geomorphological processes such as hillslope diffusion (e.g., Munch et al., 2022; Sternai, 2020) and fluvial erosion (Nettesheim et al., 2018; Ueda et al., 2015) remains outside the scope of our study.

As for the thermal boundary conditions, we applied a fixed value of 0°C at the upper boundary and a horizontal heat flux of zero across all vertical boundaries. The temperature and vertical heat fluxes can vary along the lower boundary, which is not only kinematically but also thermally permeable. This implies a constant temperature condition at ∼300 km below the bottom of the model box (Gerya et al., 2008; Li et al., 2013).

3.3. Modeling Procedure

The main control parameters of our study are (a) the obliquity angle of the passive margin (α), (b) the age of the subducting oceanic plate (t_{slab}), (c) convergence velocity (u_c), and (d) the presence of a microcontinent parallel to the original passive margin (Table 1). Since running 3D models is computationally expensive and time consuming, we did not attempt to perform a series of experiments covering all possible combinations of control parameters. Instead, we systematically changed one parameter and kept all others as in the "reference" model. This approach makes it possible to reduce the computational effort while extending the value ranges of the tested parameters. With this strategy in mind, we begin with a reference experiment (model **1**) characterized by an obliquity angle (α) of 15°, an oceanic plate age (t_{slab}) of 40 Ma, and a convergence velocity (u_c) of 4.5 cm yr^{-1}, which is defined by the horizontal push on the right side of the moving continental plate (Figure 1). Thereafter, the influence of passive margin obliquity angle (α) is tested by increasing/decreasing it in a step of 7.5° (following the earlier study by Andrić-Tomašević et al., 2023) with respect to the reference value of 15° (α is 0°, 7.5°, and 22.5°;

Table 1
Control Parameters of the Numerical Experiments

	Model parameters			
Model No	Passive margin obliquity angle, α (°)	Oceanic plate age, t_{slab} (Ma)	Convergence velocity, u_c (cm yr^{-1})	Microcontinent (no/yes)
1	15	40	4.5	No
2	*0*	40	4.5	No
3	*7.5*	40	4.5	No
4	*22.5*	40	4.5	No
5	15	*20*	4.5	No
6	15	*60*	4.5	No
7	15	*80*	4.5	No
8	15	40	*3.0*	No
9	15	40	*1.5*	No
10	15	40	*0.5*	No
11	*0*	40	4.5	*Yes*
12	*7.5*	40	4.5	*Yes*
13	15	40	4.5	*Yes*

Note. Parameter values that differ from those of reference model **1** are highlighted in italics. Three additional experiments: (a) model **14**: obliquity not of the passive margin but of the subduction zone (angle of 22.5°); (b) model **15**: no brittle and ductile weakening; (c) model **16**: no ductile weakening.

models **2**–**4**). Similarly, the thermal age of the subducting oceanic plate (t_{slab}) is changed in a step of 20 Ma from the value of the reference experiment (i.e., 40 Ma) to 20, 60 and 80 Ma (models **5**–**7**). Subsequently, to examine the effects of convergence velocity (u_c), we perform several experiments with values that are lower than in the reference experiment (4.5 cm yr^{-1}): 3.0, 1.5, and 0.5 cm yr^{-1} (models **8**–**10**). It is well known that in natural collisional settings, the presence of a small continental block (microcontinent) extending along the passive margin can add complexity not only to the architecture of the original passive margin but also to the resulting collisional orogen (Eskens et al., 2024), potentially affecting the processes of slab breakoff and tear propagation (Gün et al., 2021; Handy et al., 2010). We therefore complete our modeling set with experiments containing a microcontinent for both convergence-perpendicular (i.e., α is 0°; model **11**) and oblique passive margin (i.e., α is 7.5° and 15°; models **12**–**13**). Furthermore, in some collisional settings, the active rather than the passive margin might initially be oblique (e.g., Apennines; Rosenbaum et al., 2008). To investigate the effects of the obliquity of the active margin we run another model with an obliquity angle of 22.5° on the active margin side (model **14**). Finally, to understand how rheological weakening mechanisms control slab breakoff and tearing, we conduct two further experiments, in which the effects of brittle (Gerya et al., 2015; Huismans & Beaumont, 2003; Koptev et al., 2021) and ductile (Bercovici & Ricard, 2012; Gerya et al., 2021; Mulyukova & Bercovici, 2017) weakening (model **15**) and only ductile weakening (model **16**) are excluded.

4. Results

4.1. Reference Experiment (Model 1)

4.1.1. General Aspects

Subduction of the oceanic lithosphere beneath the right continental plate begins along the initially prescribed weak zone (Figure 1). After ∼4 Myr of model evolution, the ongoing subduction process self-consistently produces a narrow and deep trench (Figure 2a-ii) with a ∼5.5 km deep depression, as shown by the swath topography profile taken along the trench (Figure 2a-iii). As subduction progresses, the oceanic slab rolls back faster than the overriding plate advances. This leads to a decoupling of the subducting oceanic plate from the overriding continental plate (Figures 2b-i and 2f) and to an upwelling of asthenospheric material that replaces the lithospheric mantle in the decoupled region (Figures S1d and S1e in Supporting Information S1). Importantly, the decoupling of the plates develops faster on the back side of the subduction zone (see x-parallel section S3 at y = 820 km)

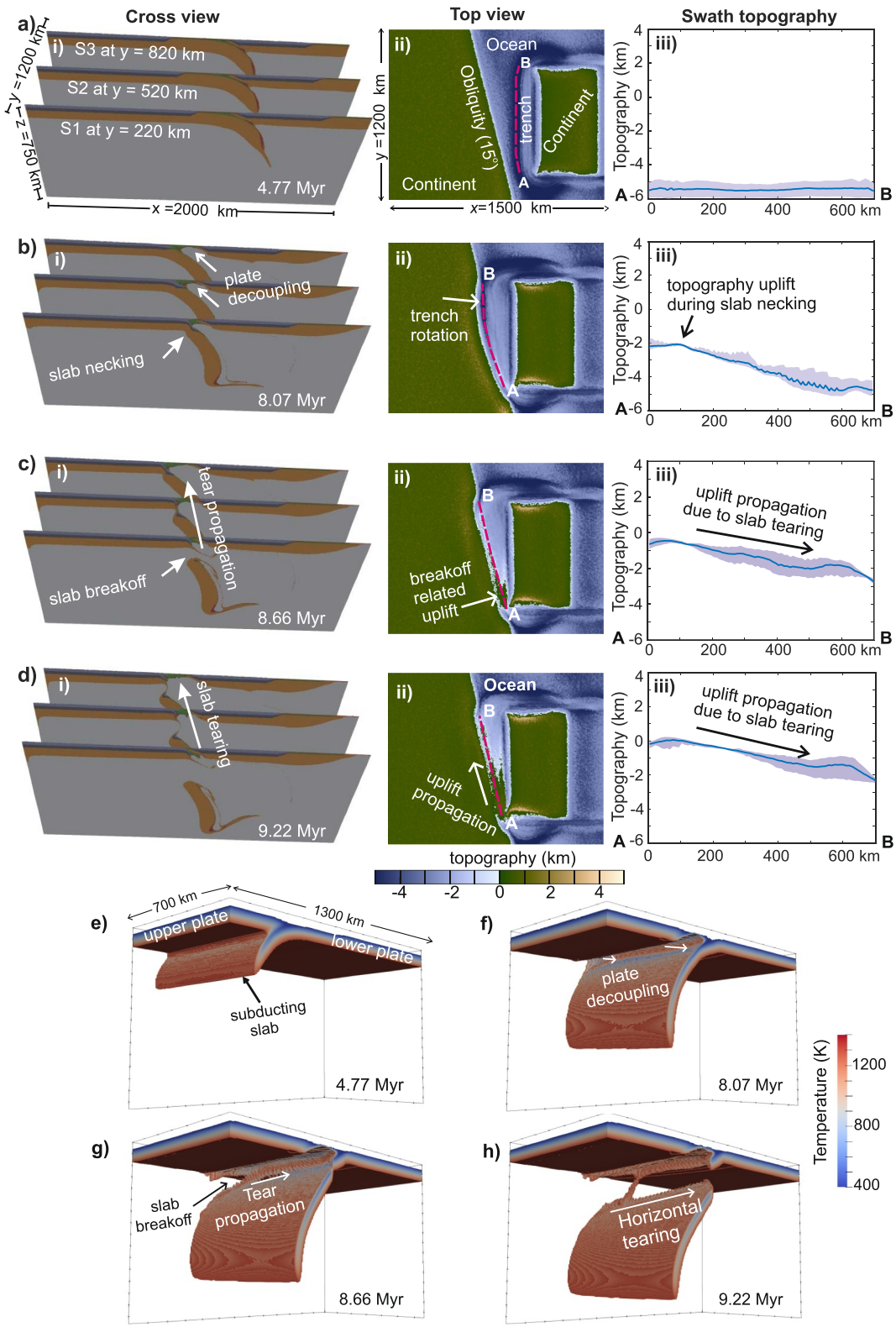

Figure 2.

compared to its front side (section S1 at y = 220 km). This causes a progressive anticlockwise rotation of the trench toward an orientation parallel to the oblique passive margin (Figure 2b-ii). Such asymmetry of slab roll-back and the resulting rotation of the trench are known to be driven by the lateral gradient in mantle return flow (Balázs et al., 2021) and momentum forces (Lallemand et al., 2008; Li & Gurnis, 2023), due to the obliquity not only of the passive (as in our case) margin (Boonma et al., 2023), but also of the original subduction zone (Andrić-Tomašević et al., 2023; Malatesta et al., 2016).

Simultaneously with the trench rotation (Figure 2b-ii), the left continental plate begins to enter the subduction zone in the front part (section S1), while oceanic subduction continues in the back part (section S3) as a consequence of obliquity of the passive margin (Figure 2b-i). The onset of continental subduction in the model can be recognized by the incipient downward movement of the upper (light blue) and lower (dark blue) continental crust (Figure 2b-i). However, the positive buoyancy of the continental crust prevents it from sinking deep into the mantle, while the attached oceanic slab subducts continuously due to its negative buoyancy. This results in localization of the extensional deformation (i.e., slab necking) at the transition from oceanic to continental plate (at 8.07 Myr after model start). The slab necking is quickly followed by the detachment (or breakoff) of the oceanic part of the plate at a depth of ∼120 km (Figure 2c-i), which in turn is reflected at the surface in an uplift of ∼1.5 km (from −2 to −0.5 km; Figures 2b-iii and 2c-iii) in this segment of the model (section S1). Given the slab breakoff in the front part, slab pull force in the middle and back segments of the subduction zone increases due to the additional slab load coming from the adjacent hanging slab (Figure 2g). As a result, slab breakoff propagates rapidly and inexorably along the former passive margin from section S1 through S2 (Figure 2c-i) and finally to S3 (Figure 2d-i), a process termed "horizontal tearing" (Figures 2g and 2h). Since the time of slab tearing from the beginning of the breakoff (∼8.1 Myr; Figure 2b-i) to the complete detachment of the entire slab (∼9.2 Myr; Figure 2d-i) is ∼1.1 Myr and the original length of the former passive margin is ∼822 km, the rate of tearing can be estimated at ∼75 cm yr^{-1}. It is also important to note that the detachment of the oceanic slab is not triggered by an early continental collision, as usually expected (e.g., Duretz et al., 2011; Gerya et al., 2004), but only by the onset of subduction of the continental part of the subducting plate beneath the fore- and back-arc domain formed during the previous processes of trench retreat and decoupling of the plates. Therefore, in our model, the slab breakoff and tearing appear to precede continental collision *sensu stricto*.

The horizontal tearing of the slab leads to along-strike migration of breakoff-induced uplift of the relief (R_{tear}) in the regions where the oceanic plate has already detached, while the topography remains relatively low where the slab rupture does not yet occur (Figure 2c-iii). When the laterally propagating slab tear finally reaches the back side (section S3) of the subduction zone (Figure 2d-i), the gradient of the surface topography along the trench-parallel profile A–B (middle panels of Figures 2a–2d) is still present (Figure 2d-iii): on the front side R_{tear} is ∼5.5 km (uplift from −5.5 to 0 km at point A), because the slab breakoff started there first, whereas on the back side R_{tear} is only ∼3.5 km (uplift from −5.5 km to −2 km at point B), as the uplift phase caused by the slab rupture begins later and is not yet completed in this area.

The phase of oblique continental collision (Figures 3a–3c) begins ∼1 Myr after the completion of slab tearing. Similar to R_{tear}, the modeled relief uplift driven by continental collision (R_{col}) gradually propagates along-strike from front to back side. Together with the pre-collision topographic gradient due to heterogeneous R_{tear} (Figure 2d-iii), this result in a strong contrast in cumulative relief uplift (R_{cum}), which varies from ∼8.5 km (uplift from −5.5 to 3 km near point A) to ∼4.5 km (uplift from −5.5 km to −1 km at point B) at 12.10 Myr (Figure 3b-iii), when the migration of the collision has not yet reached its ultimate back-side point (Figure 3b-i). It thus appears that along-strike gradient in the surface uplift and resulting mountain topography not only persists during the continental collision, but becomes even more pronounced (compare Figures 2d-iii and 3b-iii). However, in the terminal stage of collision propagation ∼2 Myr later (Figure 3c-i), the R_{cum} gradient reduces and a broad, ∼3 km-high plateau forms over most of the lateral extent of the resulting orogenic belt (Figure 3c-iii). Remarkably, the final orientation of the collision zone is almost exactly parallel to the y-axis

Figure 2. Reference model **1**: plate decoupling and slab tearing phase (∼5–9 Myr). (a–d) Left panels (i): 3D view of the compositional field along the three cross sections S1, S2, and S3, taken at y = 220, 520, and 820 km, respectively. The color code for the rock composition is the same as in the legend of Figure 1. Middle panels (ii): map view of the modeled surface topography. Right panels (iii): along-trench swath topographic profile (swath width of 40 km), marked as a pink dashed line on the map of the corresponding middle panel. (e–h) 3D view of the bulk of the model volume bounded by the 400 and 1,400 K temperature iso-surfaces, showing the most important geometric features of the downgoing plate, including the onset of slab breakoff and subsequent tearing.

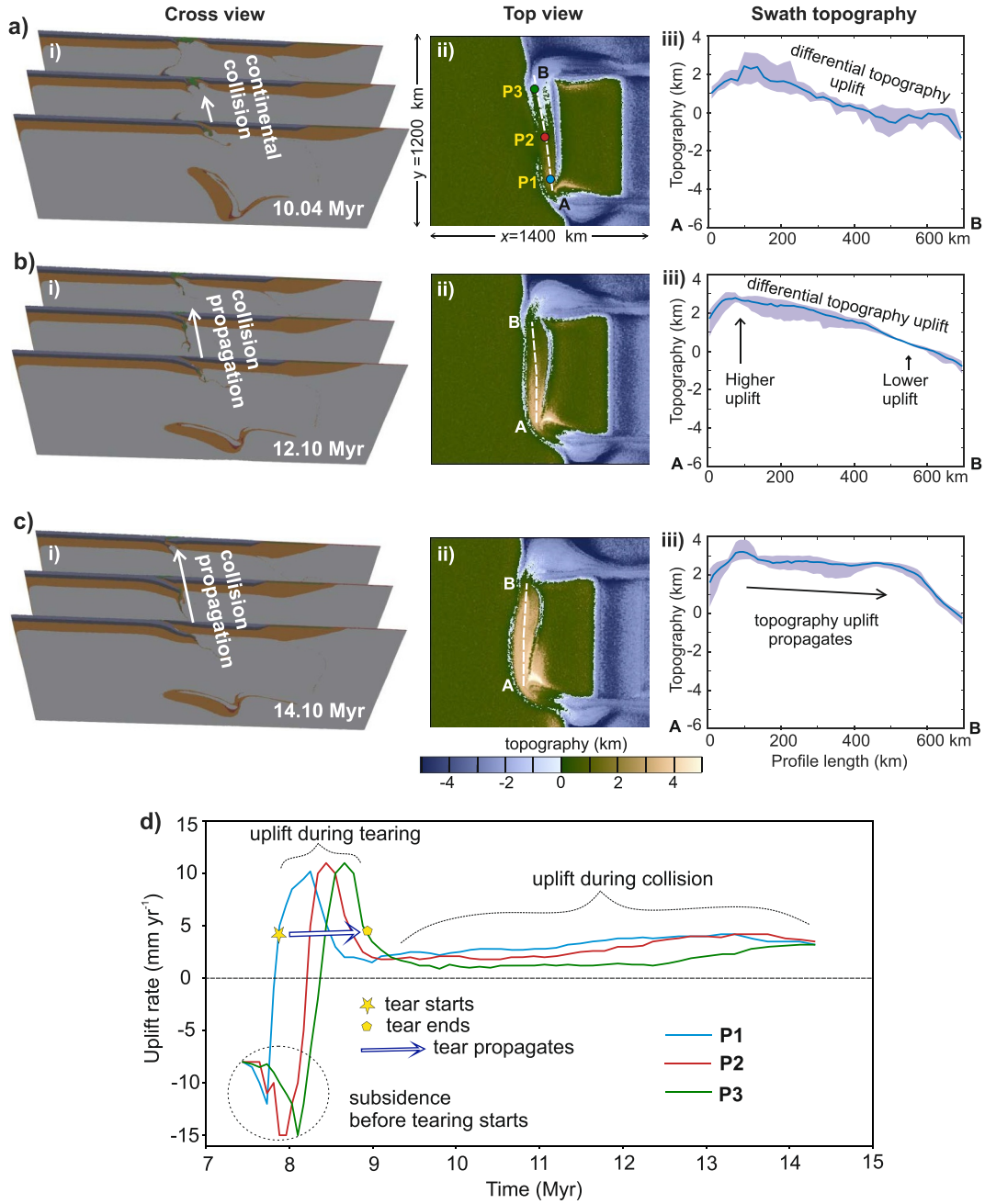

Figure 3. Reference model **1**. (a–c) Phase of oblique continental collision (~10–14 Myr). Same representation and conventions as in Figures 2a–2d. (d) Full evolution of surface uplift rate, tracked at points P1, P2, and P3 in the front, middle, and back segments of an initially passive margin, as indicated in panel (a-ii).

(Figure 3c-ii) or, in other words, perpendicular to the horizontal velocities permanently ensuring the process of plate convergence (Figure 1). It can therefore be seen that despite the complexity of a system development, which is caused by irregularities in the initial conditions (in our case, the obliquity of the passive margin), the final state of a system is essentially determined by the boundary conditions (in our case, the continental push applied parallel to the *x*-axis).

4.1.2. Evolution of Topographic Uplift Rate During Slab Tearing and Differential Collision

To analyze the spatial and temporal variations in the surface response to the geodynamic processes reproduced in reference model **1**, we tracked the topographic uplift rate for the period from just before the onset of slab tearing (7.5 Myr) to the completion of continental collision (14.5 Myr) for the three points P1, P2 and P3 (Figure 3d), which are located in different segments (front, middle, and back) of the initially passive margin (Figure 3a-ii).

Prior to the initiation of slab tearing, uplift rates at all three points are negative, with a range of values between −8 and −12 mm yr^{-1}, indicating that the entire former passive margin is experiencing extension induced by the flexural subsidence due to the influence of slab pull force from the adjacent oceanic plate (Dai et al., 2024). However, with the onset of slab tearing at ∼8.16 Myr at the front point P1 (where slab breakoff first started), subsidence rapidly switches to uplift, reaching a rate of up to ∼10 mm yr^{-1} within less than 0.5 Myr. In contrast, the middle point P2 continues to subside during the same time period, even at a higher rate of up to −15 mm yr^{-1}, due to the additional slab pull from the neighboring segment of the hanging slab. For the same reason, the subsidence at the back point P3 also accelerates (up to the same rate of −15 mm yr^{-1}), when the middle point P2 is about to rise (Figure 3d). Such along-strike shift in the increased subsidence rate, which precedes shortly the propagation of slab breakoff, is known as depocenter migration (Meulenkamp et al., 1996; van der Meulen et al., 1998).

During the slab tearing phase, the high uplift rate migrates along the former passive margin together with the propagation of slab rupture. The uplift rate at all three points (P1, P2, and P3), which initially increases to ∼10 mm yr^{-1}, is then abruptly reduced to ∼2 mm yr^{-1} as the slab breakoff is locally completed on the way of its propagation. The time lags between the maxima of the uplift rates at the traced points are ∼0.1–0.2 Myr, while the total time of slab tearing is ∼1.1 Myr (Figure 3d), as mentioned above.

During the subsequent collision phase, the topographic uplift rate does not exceed 4 mm yr^{-1}. Due to the obliquity of the margin, the collision began at the front (point P1) and then propagated toward the back (point P3) side from ∼8.77 to ∼12.65 Myr. The resulting duration of the collision propagation (∼4 Myr), together with the length of the collision zone (∼822 km), yields a propagation velocity for the differential collision and the associated topographic uplift of ∼20.6 cm yr^{-1}, that is almost four times slower than the tear propagation, estimated as ∼75 cm yr^{-1} (see above). Importantly, the topographic uplift rate at points P2 and P3 was initially lower than at point P1, because the collision in the middle and back segments started later than in the front part. However, as the collision propagates along-strike over time, the topographic uplift rate also increases at points P2 and P3, resulting in similar values of uplift rate of ∼4 mm yr^{-1} in all three collision segments at ∼14.5 Myr (Figure 3d).

4.2. Effects of Passive Margin Obliquity (Models 2–4)

To understand the influence of the initial obliquity angle of the originally passive margin (α) on the evolution of the system, including along-strike propagation of R_{tear} and R_{col}, we performed models **2**–**4** (Figure 4), where α has variable values (0°, 7.5°, and 22.5° instead of the reference 15°), while all other parameters are unchanged compared to reference model **1** (Table 1).

A non-oblique geometry of the passive margin (model **2**; $\alpha = 0°$, $t_{slab} = 40$ Ma, $u_c = 4.5$ cm yr^{-1}) leads to a simultaneous onset of continental subduction along its entire length (Figure 4a and Figure S2 in Supporting Information S1). As a result, slab breakoff and associated surface uplift initiate concurrently along strike (Figure 4d and Figure S2 in Supporting Information S1), so that the velocity of slab tearing is infinite (Figure 4g). The same applies to the subsequent collision phase, in which the topography continues to grow synchronously along the newly formed collision zone (Figures 4a and 4d and Figure S2 in Supporting Information S1). However, even a relatively small obliquity as in model **3** ($\alpha = 7.5°$) causes progressive along-strike migration of slab rupture (slab tearing) and differential collision propagating from front to back side (Figure 4b), generally similar to the reference case described above (see Section 4.1.1). Our parametric analysis shows a systematic decrease in slab tearing velocity with increasing initial obliquity of the passive margin (Figure 4g). In particular, the obliquity of 7.5° (model **3**) gives a propagation velocity of the slab tear (∼118 cm yr^{-1}) that is about three times higher than in model **4** (∼38 cm yr^{-1}), where the margin obliquity is 22.5° (Figure 4g). Accordingly, breakoff-induced uplift of the relief (R_{tear}) also propagates more slowly along the margin with a higher obliquity: the total duration of its along-strike migration is ∼0.7 Myr in model **3** ($\alpha = 7.5°$), which increases to ∼2.2 Myr in model **4** ($\alpha = 22.5°$). As for the maximum rate of vertical topographic uplift, it reaches up to ∼14 mm yr^{-1} in models **2** and **3** ($\alpha = 0°$ and 7.5°; Figures 4d and 4e), which is remarkably higher than in experiments with stronger margin obliquity such as

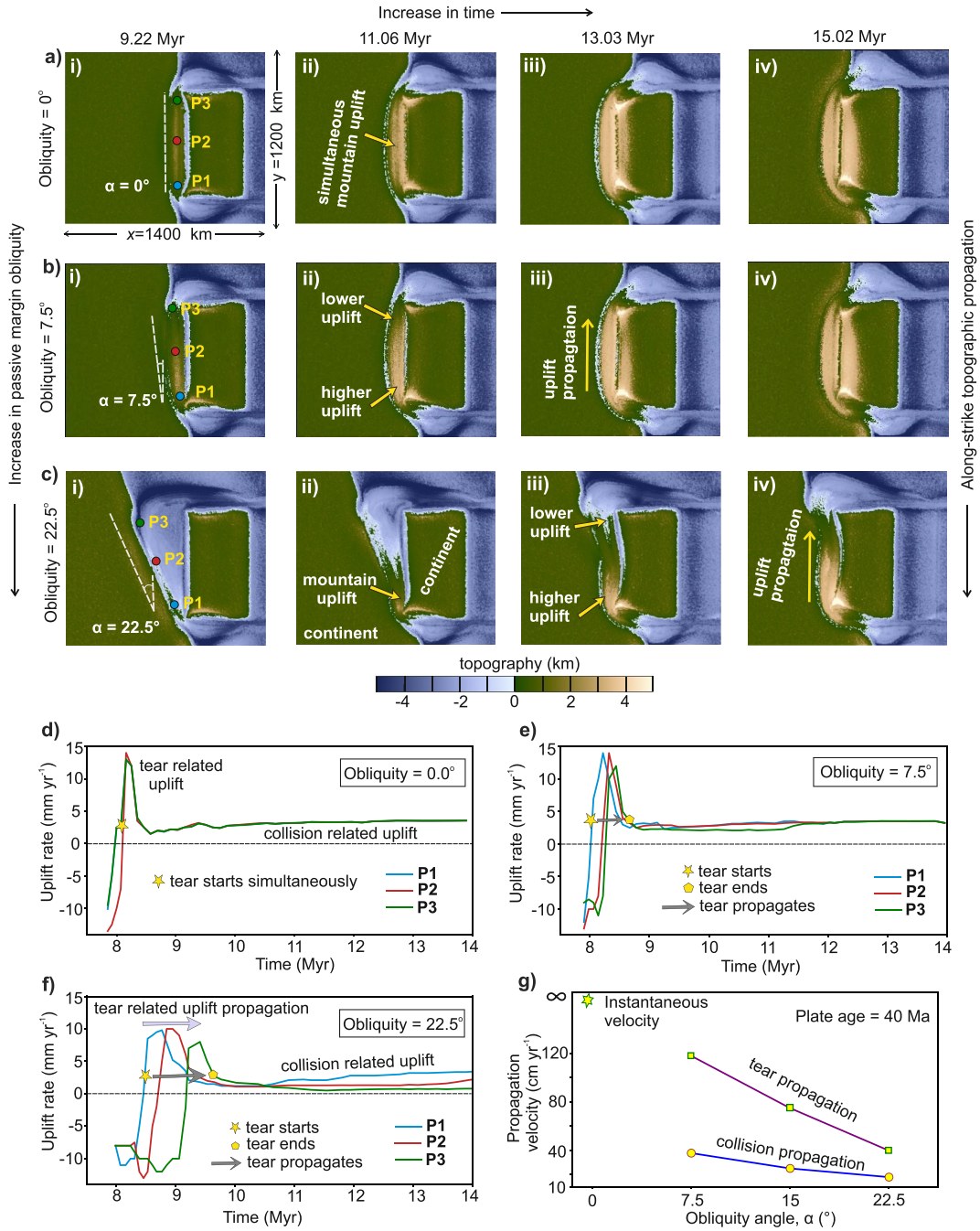

Figure 4. Models **2**–**4**, investigating variations in obliquity angle (α; Table 1). (a–c) Map view of the evolution of the modeled surface topography. (d–f) Evolution of surface uplift rate in the front, middle, and back segments of an initially passive margin. The corresponding points P1, P2, and P3 are indicated in panels (a–i), (b–i), and (c–i). (g) Modeled estimated slab tear propagation and collision propagation velocities as a function of obliquity angle, where plate age is kept constant at 40 Ma. Note that for non-oblique margin ($\alpha = 0°$) both along-strike tear propagation and collision propagation velocities are instantaneous.

reference model **1** (α = 15°) and model **4** (α = 22.5°), whose maximum uplift rate is only ~10 mm yr^{-1} (Figures 3d and 4f).

In all models, after the end of the slab tearing phase, the uplift of the topography is driven by the continental collision *sensu stricto*, that is, the impingement between two converging continental plates. The obliquity of the

passive margin causes this impingement to occur first on the front side and then spread along-strike to the back side. Therefore, we consider the along-strike length of the passive margin as the collision propagation length. Due to variations in passive margin obliquity, the length of collision propagation also varies in models **1–4**. Based on the analysis of the collision-induced relief uplift (R_{col}), which is characterized by along-strike propagation from the front to the back segment of the collision zone (i.e., from point P1 to point P3; Figures 4a–4c), we estimated the duration of the collision migration as well as the velocity of this process (Figure 4g). In model **3** with $\alpha = 7.5°$, collision propagation lasts ∼2.35 Myr (from ∼8.75 to ∼11.10 Myr). For a given margin length of 806 km, this results in propagation velocity of ∼34 cm yr^{-1} that is faster compared to the reference model **1** ($\alpha = 15°$), where it is only ∼20 cm yr^{-1} (Section 4.1.2). An even slower propagation (∼13 cm yr^{-1}) is detected in model **4** ($\alpha = 22.5°$), where the collision starts at 9.2 Myr and its propagation terminates at 15.8 Myr, while the original distance between points P1 and P3 is 865 km.

4.3. Effects of Oceanic Plate Age (Models 5–7)

In experiments **5–7**, we varied the thermal age of the oceanic plate from 20 to 80 Ma, while keeping all other parameters as reference (i.e., $\alpha = 15°$ and $u_c = 4.5$ cm yr^{-1}), to explore the impact of the associated variations in buoyancy and strength of the oceanic lithosphere (Burov, 2011; Turcotte & Schubert, 2002) on the timing of slab breakoff and the velocity of slab tearing.

The breakoff of the youngest oceanic plate (model **5**; 20 Ma) initiates at ∼8.8 Myr (Figure 5a-ii), almost 1 Myr later than the slab rupture in model **6** (∼7.9 Myr; Figures 5b-i), in which an oceanic lithosphere is older (60 Ma). The reason for this is that the older oceanic plates are heavier and therefore exert higher slab pull forces, leading to an earlier onset of slab detachment (Figure 5d). In addition, with increasing age of the oceanic plate, its rheology (i.e., effective viscosity) also becomes stronger (Figure S3 in Supporting Information S1). As a result, model **7** with the oldest oceanic lithosphere (80 Ma; Figure 5c) shows a significantly slower lateral propagation of slab breakoff (velocity of ∼55 cm yr^{-1}), compared to the tearing velocity of ∼70–80 cm yr^{-1} detected in other experiments (Figure 5e). Importantly, slow tear migration in the experiment with the oldest oceanic slab (model **7**; 80 Ma) is also characterized by extremely shallow levels (∼50 km depth) of plate necking and detachment in the central (Figure 5c-ii) and back (Figure 5c-iii) segments of the subduction zone. Moreover, this shallow breakoff does not seem to occur in the slab *sensu stricto*, but in the continental part of the descending plate, which is not even involved in the subduction (Figure 5c).

To summarize, a higher oceanic plate age generally leads to a slower along-strike propagation of slab tear (Figure 5e), but to an earlier onset of slab breakoff (Figure 5d). However, the model **7** with the oldest oceanic plate (80 Ma; Figure 5c) is an exception, as the high slab strength in this case causes a delay in the initial breakoff in the front part of the model, compared to the model **6** with the relatively younger (60 Ma; Figure 5b) age of the plate (Figure 5d). It is also important to note that in the adjacent central and back segments the model **7** ($t_{slab} = 80$ Ma) does not show slab rupture at the transition between the oceanic and continental plates, as is the case in all other experiments. In contrast, here the localization of the shallow slab necking and tearing is directed toward the continental domain of the subducting plate (Figure 5c, segments S2 and S3).

4.4. Effects of Convergence Velocity (Models 8–10)

In nature, the beginning of continental collision is known to decrease the velocity of plate convergence (Boutoux et al., 2021; Maiti et al., 2021). In experiments **8**, **9**, and **10** (Figure 6), we examine the effects of a syn-collisional reduction in the convergence velocity (u_c), which was gradually decreased from the reference value of 4.5 cm yr^{-1} to 3, 1.5, and 0.5 cm yr^{-1} shortly after the collision onset at ∼8.8 Myr of model time (see Figure S4 in Supporting Information S1).

The results reveal that the along-strike propagation of collision-induced relief uplift (R_{col}) from the front (point P1) to the back (point P3) of the orogenic belt (Figures 6a–6c) is systematically faster in the models with higher syn-collisional convergence velocity (Figures 6d–6g). In particular, for u_c of 3 cm yr^{-1}, R_{col} reaches point P3 at ∼14.5 Myr, indicating a propagation period of ∼5.7 Myr, which increases to ∼12.7 Myr and even to >30 Myr in the experiments with u_c of 1.5 cm yr^{-1} and 0.5 cm yr^{-1}, respectively. The corresponding rates of R_{col} propagation ∼14.7, ∼6.5, and ∼2.3 cm yr^{-1}, while the highest value (∼20.6 cm yr^{-1}) is expectedly belongs to the reference model **1** with unreduced u_c of 4.5 cm yr^{-1} (Figure 6g).

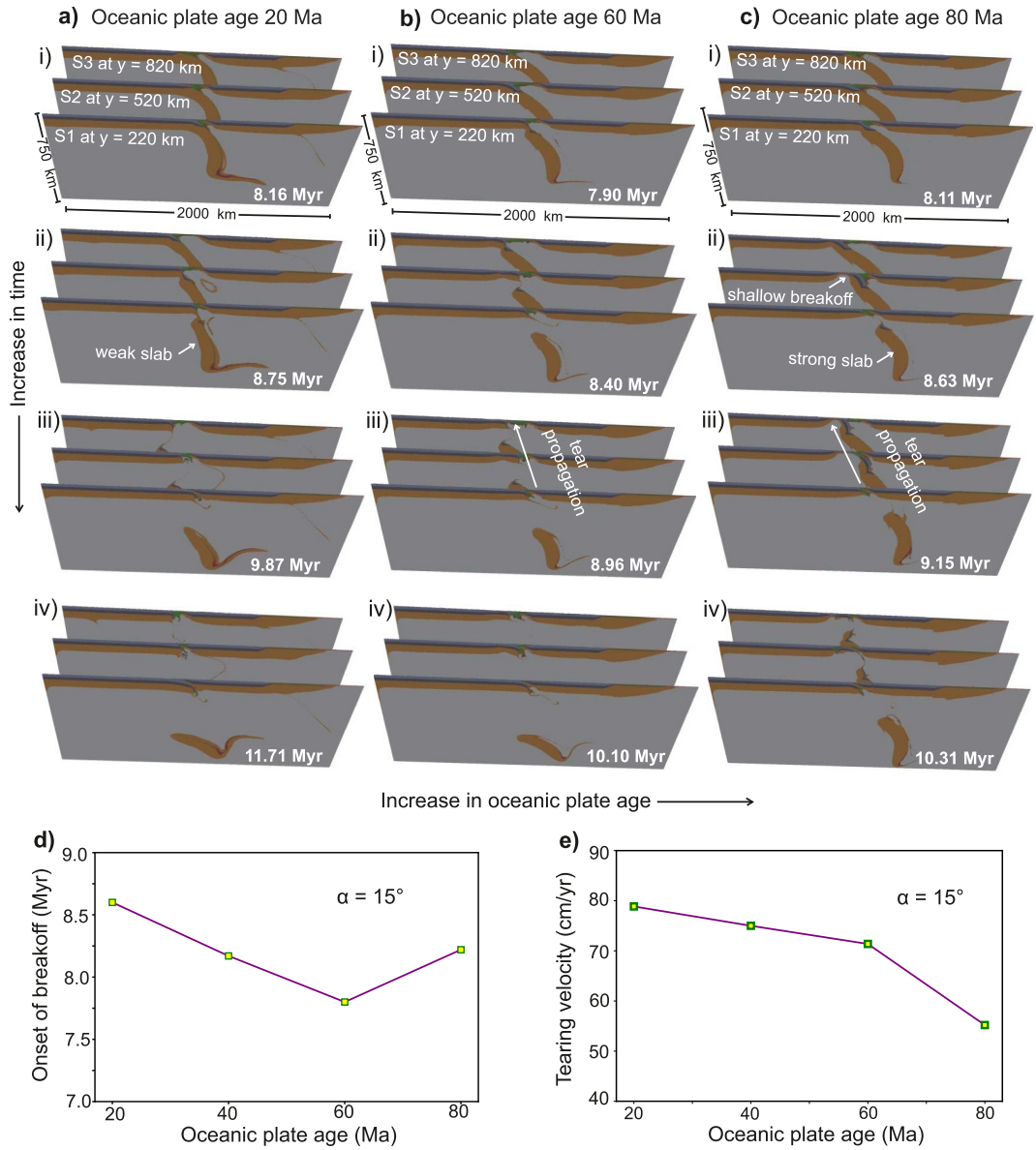

Figure 5. Models **5**–**7**, investigating variations in oceanic plate age (t_{slab}; Table 1). (a–c). 3D view of the evolution of the compositional field. (d) Modeled time of the onset of slab breakoff as a function of oceanic slab age. (e) Modeled velocity of slab tearing as a function of oceanic slab age.

4.5. Effects of Microcontinental Block (Models 11–13)

In natural continental collisional settings, originally passive margins often exhibit various geometric irregularities, such as weakly thinned continental blocks that were separated from the main continent during the previous phase of extension (Gül et al., 2015; Koptev et al., 2019; Lash, 1998; Manatschal & Müntener, 2009; Mohn et al., 2014; Müller et al., 2001). To explore the impact of such irregularities on slab tearing, continental collision, and associated uplift of the topography, we introduce a microcontinent between two colliding continental plates parallel to the passive margin with obliquity angles of 0°, 7.5°, and 15° (models **11**, **12**, and **13**, respectively), while maintaining an oceanic slab age of 40 Ma and a convergence velocity of 4.5 cm yr^{-1} as in the reference model **1**. Note that the microcontinent extends only over a limited segment along the front part of the oblique passive margin (Figure 1).

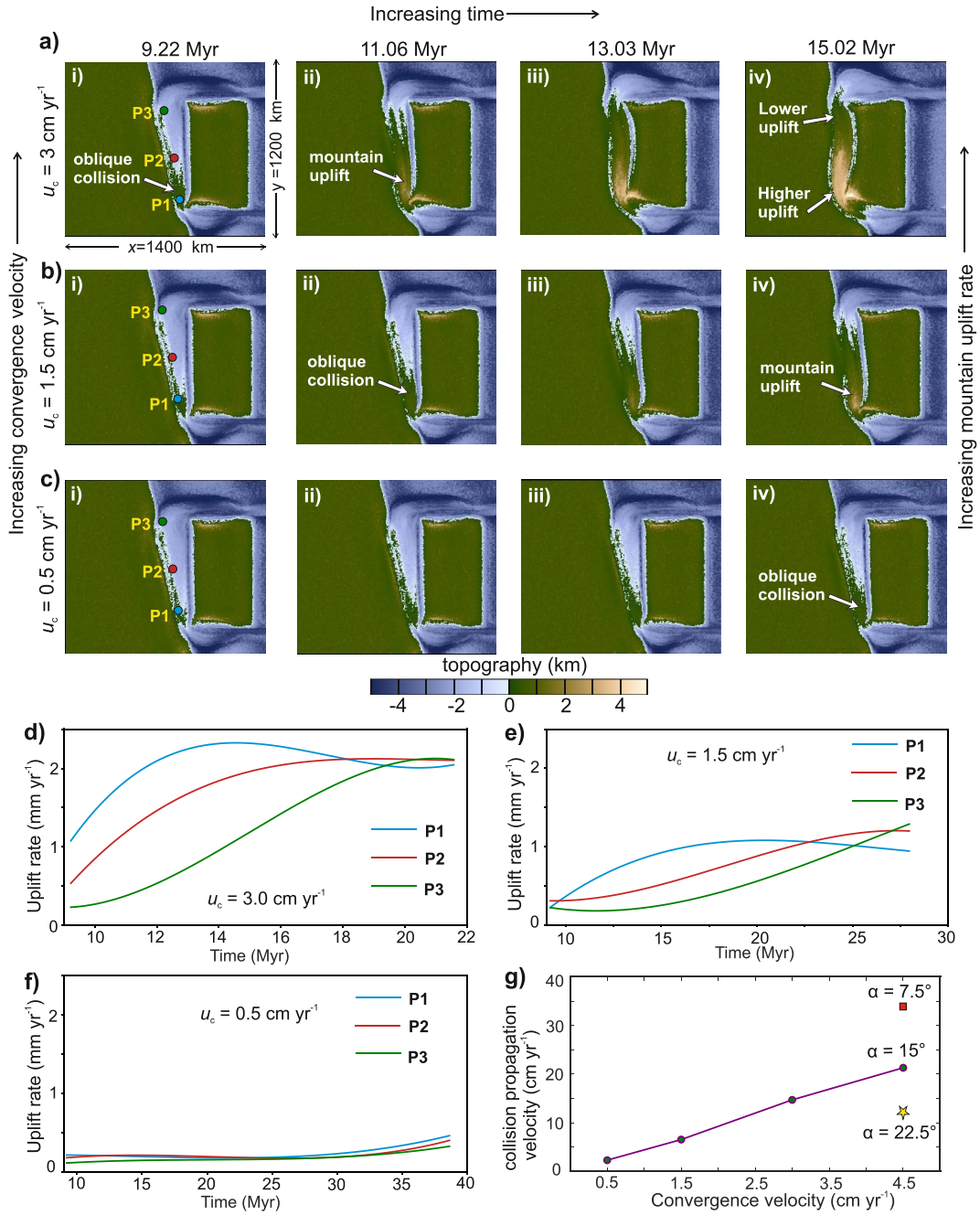

Figure 6. Models **8**–**10**, investigating variations in convergence velocity (u_c; Table 1). (a–c) Map view of the evolution of the modeled surface topography. (d–f) Evolution of surface uplift rate at points P1, P2, and P3, indicated in panels (a–i), (b–i), and (c–i), during collision phase. (g) Modeled collision propagation velocities as a function of convergence velocities. The solid line plot is for the reference model (i.e., obliquity angle $\alpha = 15°$). Note that for relative comparison, collision propagation velocities for other obliquity angles ($\alpha = 7.5°$ and 22.5°, at $u_c = 4.5$ cm yr^{-1}) are also plotted.

In contrast to all previous experiments, in which the collision phase always begins after the complete detachment of the entire oceanic plate along strike, model **11** (passive margin obliquity of 0° in the presence of the micro-continent; Figure 7) shows an earlier collision between the microcontinental block and the right continental plate (Figure 7b-ii), when the tearing of subducting slab has not yet reached its terminal point in the back segment of the convergence zone (Figures 7b-i). In other words, the presence of the microcontinent leads to a synchronous continental collision and slab breakoff, as also reported in a previous study by Gün et al. (2021). Moreover, the

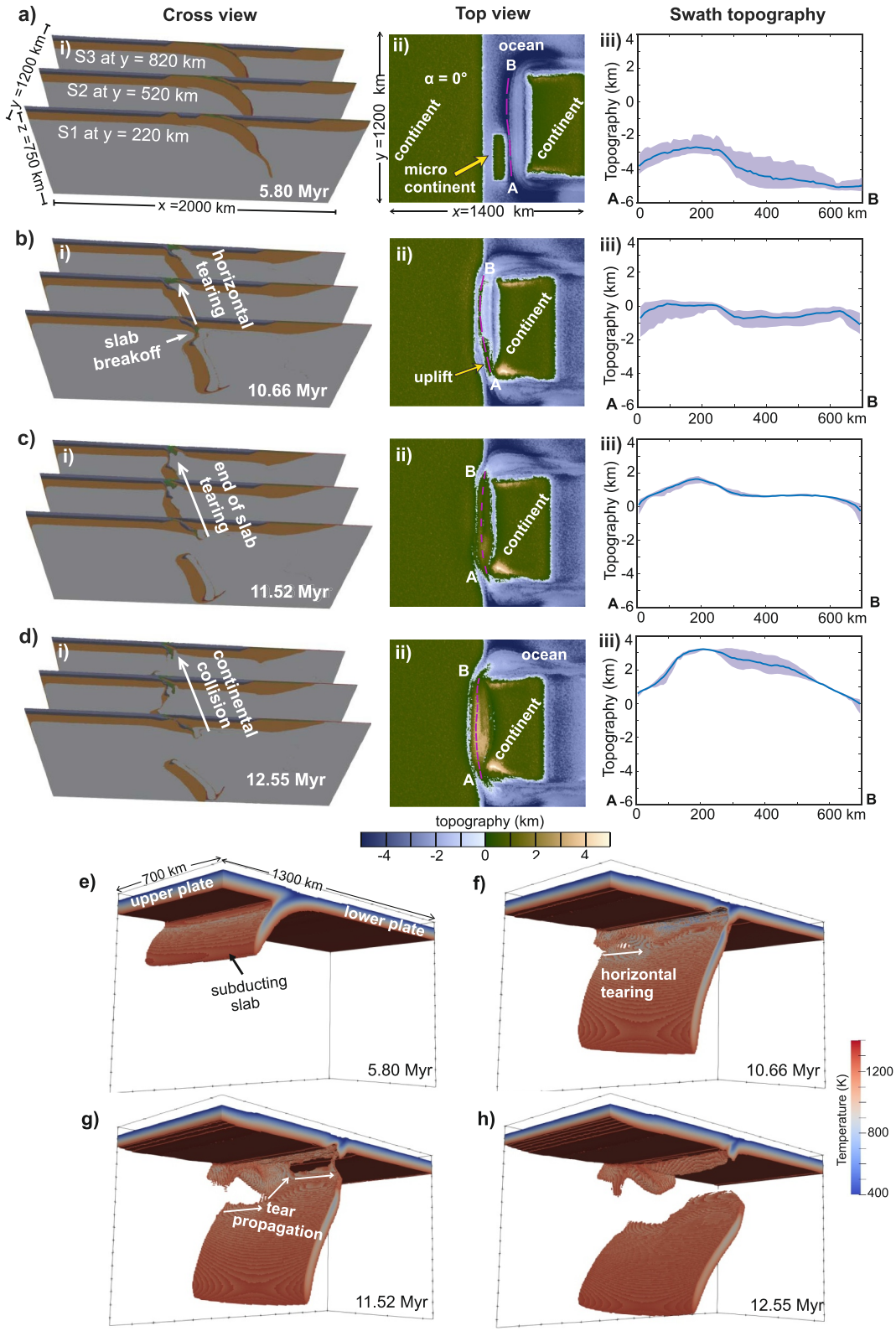

Figure 7. Evolution of model **11**, illustrating the effects of a microcontinent parallel to the non-oblique passive margin. Same representation and conventions as in Figure 2.

existence of the microcontinent appears to delay slab breakoff (by ~0.86 Myr) in the back segment compared to the front segment, which includes the microcontinent area. Considering the tear propagation length of 800 km, it gives a tearing rate of ~93 cm yr^{-1}. Note that for a non-oblique passive margin without a microcontinent (i.e., model **2**), the tear propagation was almost instantaneous (Figure 4d).

However, in case of the presence of a microcontinental block is combined with an oblique passive margin (obliquity 7.5°; model **12**, Figure 8), the system evolves differently compared to non-oblique passive margin one (model **11**). In particular, migration of the slab rupture along the oblique margin is more complex, as it includes the phase of vertical tearing (Figure 8g) along the shorter (parallel to *x*-axis) boundary of the microcontinent (Figure 8b-ii). This vertical slab tearing separates two episodes of horizontal breakoff propagation in the front and back segments of the subduction zone (Figures 8f–8h), in agreement with the recent finding that horizontal and vertical slab tearing may be different stages of the same geodynamic process even in the case of a homogeneous oceanic plate (Andrić-Tomašević et al., 2023). In model **12**, the estimated vertical tear length is ~140 km (Figure 8c-ii), while the slab tearing process is completed within ~0.6 Myr (Figures 8f and 8g). This results in a vertical tear velocity of ~23 cm yr^{-1}, which is much lower than the rate of horizontal tear propagation (~70 cm yr^{-1} or ~480 km in ~0.68 Myr). In the back segment, where the microcontent does not extend, horizontal tearing of the oceanic slab is terminated before the collision between the "primary" (left and right) continents (Figure 8d), similar to the previous models. As the collision starts much earlier in the front segment containing the continental microblock (Figure 8c-ii), the corresponding along-trench topography profile exhibits a strong asymmetry (Figure 8c-iii), which persists throughout the rest of the model (Figure 8d-iii). In model **13**, the presence of a microcontinent is combined with passive margin obliquity increased to reference value ($\alpha = 15°$). This experiment shows a very prominent vertical tearing, a longer phase of tear propagation (~2 Myr), and a more pronounced along-trench topographic asymmetry (Figure S5 in Supporting Information S1).

4.6. Effects of Trench Obliquity (Model 14) and Weakening Mechanism (Models 15–16)

In addition to the previous experiments, in which the asymmetry of the system is introduced by the obliquity of the original passive continental margin, we also performed model **14** (Figure 9), where the weak left boundary of the right continental plate (which quickly turns into a subduction zone after the start of the experiment) forms an obliquity angle of 22.5° with the left and right model boundaries, while the passive margin on the opposite side of the ocean is parallel to the *y*-axis (Figure 9a-ii).

Along-trench variations in slab rollback, characterized by a gradually increasing trench retreat velocity from front to backside, lead to an anticlockwise rotation of the subduction zone with a resulting orientation perpendicular to the convergence direction (Figure 9b-ii), similar to previous modeling studies of the oblique oceanic subduction (Andrić-Tomašević et al., 2023; Malatesta et al., 2016). The faster slab rollback in the middle and back segments of the subduction zone (Figure 9g) induces the decoupling of the oceanic plate from the overriding continental lithosphere, as seen in sections S2 and S3, in contrast to the front part (section S1), where the retreat of the trench is slower and thus compensated by the forward movement of the upper plate (Figure 9b-i). When continental collision starts in the front part (section S1; Figure 9b-i), trench rotation is already completed and the convergence zone is thus parallel to the original passive margin (Figure 9b-ii), so that continental subduction initiates simultaneously in the middle and back segments (sections S1 and S2; Figure 9b-i). Nevertheless, the slab breakoff first occurs in the collisional (front) segment and then propagates as a horizontal tear along strike (Figures 9c and 9d) with a velocity of ~53 cm yr^{-1}. Therefore, the initial obliquity of the active margin could also result in slab breakoff that progressively migrates laterally (Figure 9h) with a velocity of the same order of magnitude (tens cm yr^{-1}) as the slab tearing in the case of the originally oblique passive margin (see Figure 4g). However, the resulting gradient in topographic uplift along the orogen in the final phase of slab tearing appears to be less pronounced (compare Figures 2d-iii and 9d-iii).

Finally, to explore the role of the rheological weakening mechanisms implemented in our numerical models, we conducted additional experiments without ductile and/or brittle weakening (models **15**–**16**). The model that excludes both ductile and brittle weakening (model **15**) hinders the decoupling of subducting and overriding plates and slab breakoff (Figure S6 in Supporting Information S1). In contrast, the model without ductile weakening only (model **16**) allows decoupling of the plates, but breakoff and subsequent tearing of the slab still do not occur (Figure S7 in Supporting Information S1). In agreement with previous studies (Baitsch-Ghirardello

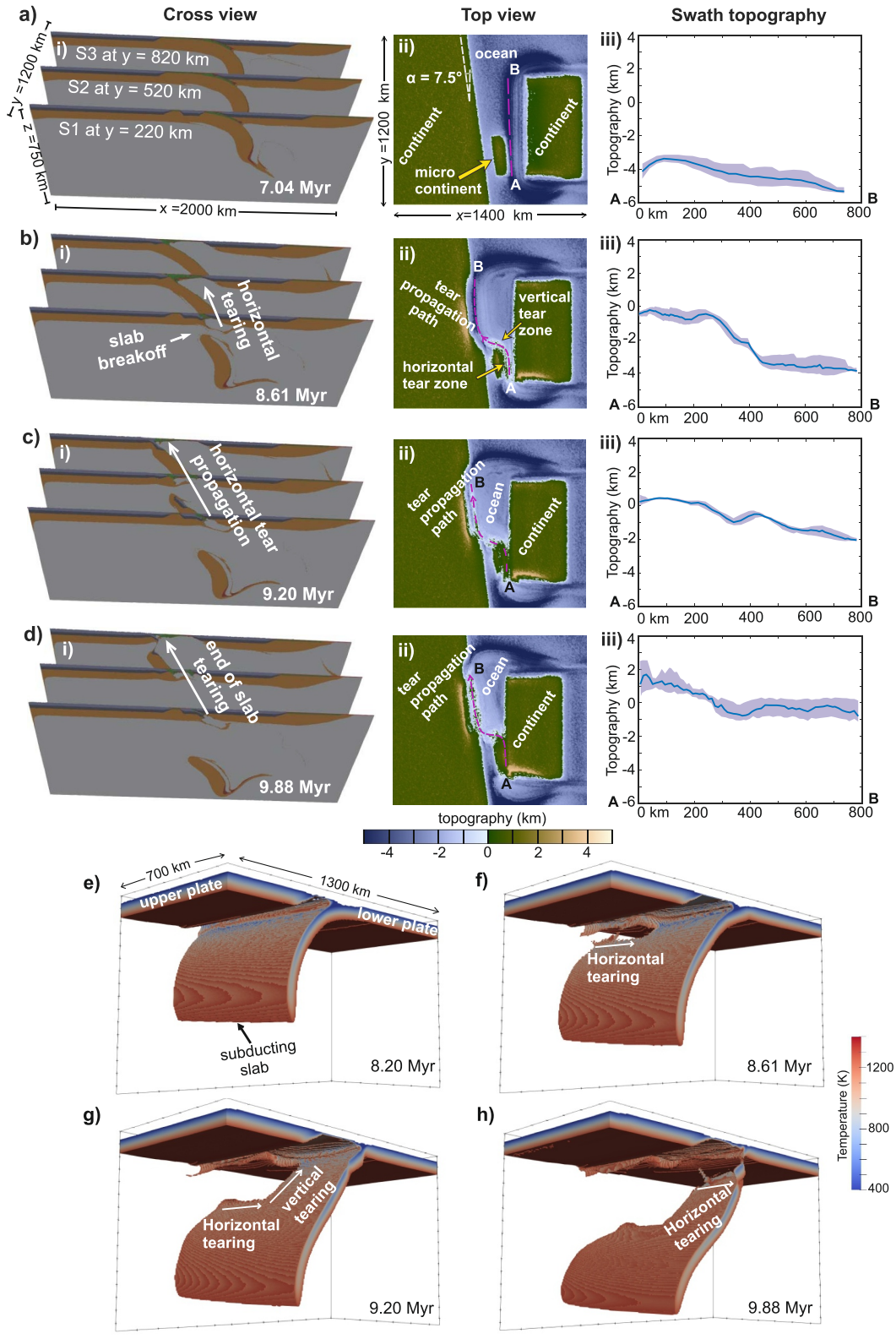

Figure 8. Evolution of model **12**, illustrating the effects of a microcontinent parallel to the passive margin with obliquity angle of 7.5°. Same representation and conventions as in Figure 2.

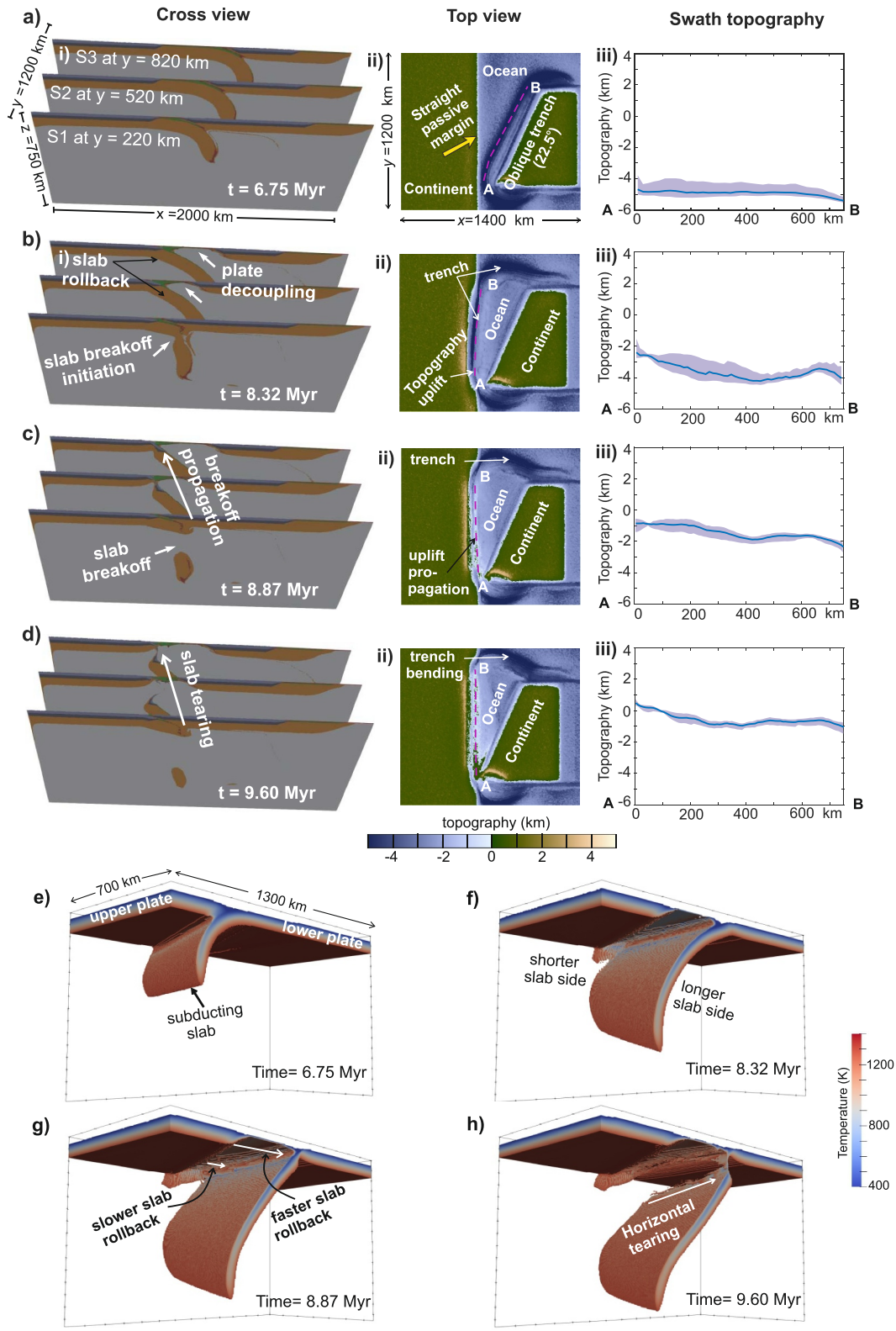

Figure 9. Evolution of model **14**, illustrating the effects of an obliquity of subduction zone. Same representation and conventions as in Figure 2.

et al., 2014; Gerya & Meilick, 2011), this underlines the importance of implementing rheological weakening mechanisms in subduction modeling.

5. Discussion

5.1. Slab Tearing and Differential Collision as a Result of Passive Margin Obliquity

5.1.1. Slab Tearing Phase

In our experiments, the subduction velocity of the oceanic plate exceeds the overall convergence velocity, leading to a rollback of the slab and a retreat of the trench with respect to the overriding plate. The retreat of the subduction zone is accompanied by an upwelling of asthenospheric material from the mantle wedge, that replaces the lithospheric mantle of the upper plate and decouples it from the downgoing slab (Figure 10a-i). Due to the obliquity of the original passive margin, that has as a geometric consequence a variable width of the oceanic plate in different model segments (Figure 1), the lateral asymmetry of the momentum force (Lallemand et al., 2008; Li & Gurnis, 2023) and mantle return flow (Balázs et al., 2021) promotes variable velocities of slab retreat along the trench (Figure 10a-i), which in turn results in a gradual rotation of the subduction zone toward an orientation parallel to the passive margin. Despite this trench rotation, the transition from oceanic to continental subduction begins first on the initially shorter side of the oceanic plate, so that slab breakoff initiates earlier there (Figure 10a-ii). As soon as slab rupture begins, it spreads rapidly in the form of horizontal tear along the former passive margin (Figure 10a-iii). This process of slab tearing is accompanied by a lateral propagation of rapid surface uplift with a vertical magnitude of up to >10 mm yr^{-1} (Figures 3d and 4d–f). A very small time delay (<0.5 Myr) between slab detachment and topographic uplift, as also found in previous studies (e.g., Duretz et al., 2011), allows to consider a migration of the slab tear and the associated topographic uplift as quasi-synchronous and with identical horizontal velocity (Figure 2).

It is noteworthy that the modeled velocity of tear propagation ranges from ∼38 cm yr^{-1} to ∼118 cm yr^{-1} (Figure 4g), which is very fast in geological time scales. These estimates are consistent with previous modeling studies (Andrić-Tomašević et al., 2023; Boonma et al., 2023; Burkett & Billen, 2010; van Hunen & Allen, 2011), that report a slab tearing rate of ∼10–130 cm yr^{-1}, depending mainly on the slab age and rheology. The depth of the slab rupture and the resulting vertical uplift of the topography (∼110 km and up to ∼10 mm yr^{-1} in reference model **1**) are also within the range of the corresponding values determined in earlier numerical modeling (e.g., Duretz et al., 2011).

According to our results, the initial obliquity of the passive margin is the most important parameter controlling horizontal velocity of slab tearing, as a change in obliquity angle from 22.5° to 7.5° increases the rate of tear migration by almost three times (from ∼38 cm yr^{-1} to ∼118 cm yr^{-1}), whereas plate boundaries perpendicular to the convergence direction (obliquity angle of 0°) cause slab breakoff to occur simultaneously along the entire trench, so that the velocity of slab tearing is infinite in this case (Figure 4g). In general, the variations in the thermal age of the subducting oceanic plate do not produce such a pronounced change in the slab tearing velocity (Figure 5e). However, the oldest slab (80 Ma) reduces the tear propagation rate to ∼55 cm yr^{-1} (compared to ∼75–80 cm yr^{-1} in other experiments with the reference obliquity angle of 15°), in agreement with previous numerical studies (e.g., van Hunen & Allen, 2011). The introduction of additional structural complexity in the form of a microcontinental body near the original passive margin (Figure 10b-i) result in a transition from horizontal tearing along the long side of the microcontinent to vertical tearing along its shorter edge (Figure 10b-ii), which is followed by another episode of horizontal breakoff propagation along the boundary of the "main" continent (Figure 10b-iii). Such a temporal and spatial transition between horizontal and vertical slab tearing as part of the continuous geodynamic process has recently been demonstrated also in simpler, non-collisional environments (Andrić-Tomašević et al., 2023).

One of the most important outcomes of our retreating collision modeling is that slab breakoff can be initiated not only by a continental collision *sensu strictro*, as in most earlier 2D (Duretz et al., 2011; Gerya et al., 2004; Magni et al., 2013) and 3D numerical modeling studies (Li et al., 2013; Menant et al., 2016; Sternai et al., 2014), but as a consequence of the transition from oceanic to continental subduction (Figure 10a-ii) beneath the fore- and back-arc domain underlain by asthenospheric material that had flowed in during the preceding phase of slab retreat and plate decoupling (Figure 10a-i). In most of our experiments, the impingement between two converging

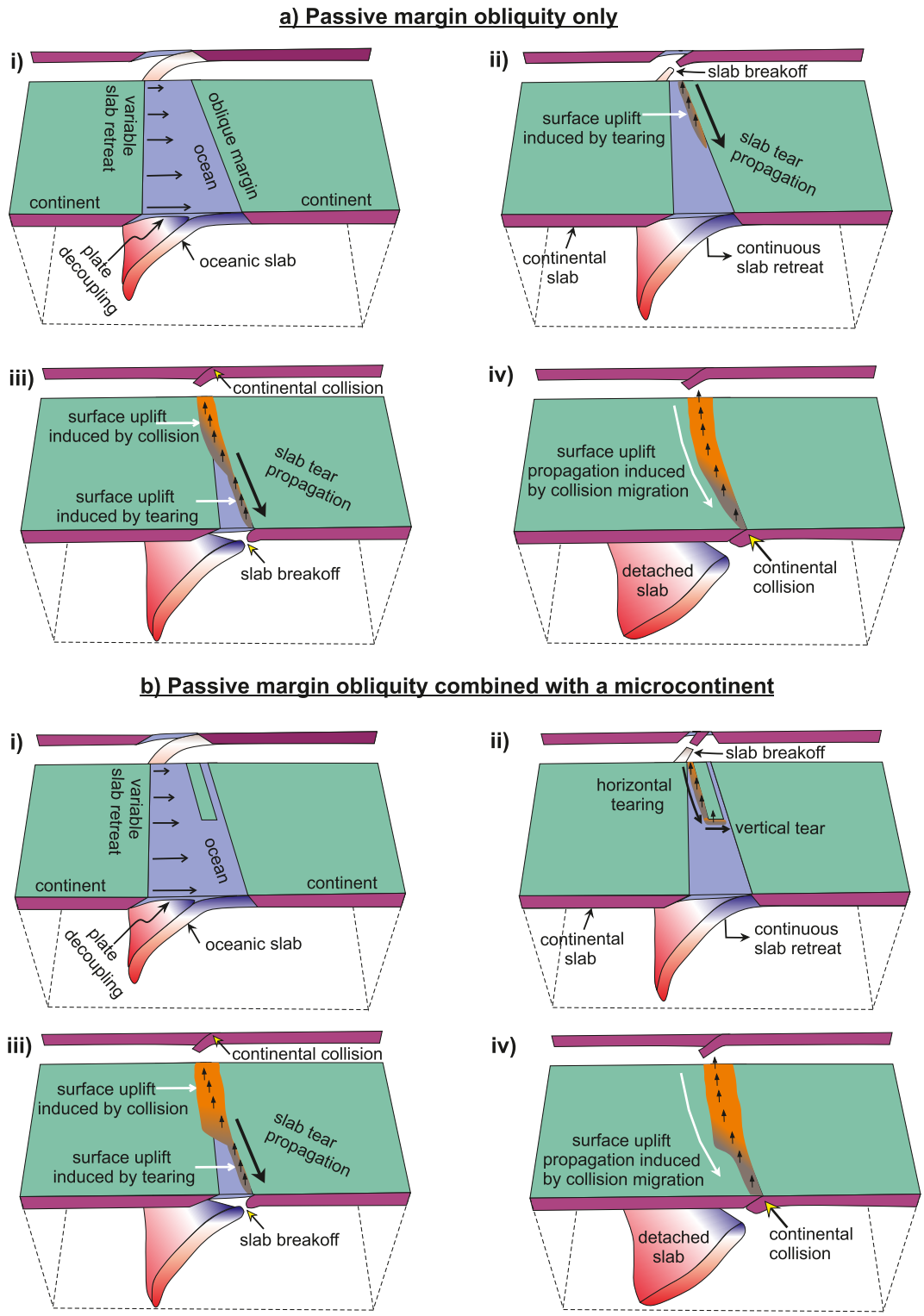

Figure 10. A schematic representation of the consequences of passive margin obliquity for the evolution of the convergent geodynamic system, including slab tearing, subsequent differential collision, and associated along-strike topographic changes in two different model scenarios: (a) obliquity of the original passive margin and (b) obliquity of the passive margin in combination with an additional irregularity in the form of a microcontinental block.

continental plates (continental collision *sensu stricto*) begins only after the completion of the slab tearing phase, when the entire oceanic plate has already been totally detached (Figure 10a-iii).

5.1.2. Differential Collision Phase

The oblique configuration of the original passive margin (Figure 10a-i) leads not only to a laterally propagating slab breakoff (Figure 10a-ii), but also to a diachroneity of the subsequent collision, which always starts on the side of the initially shorter oceanic segment (Figure 10a-iii) and then migrates along strike, following the path of the preceding slab tearing and causing an uplift of topography (Figure 10a-iv).

The vertical magnitudes of the topographic uplift rates during the phase of diachronous collision are significantly lower than those during the slab tearing (Figures 3d and 4d–4f). For example, in reference model **1** with an obliquity angle of 15° and a constant convergence velocity of 4.5 cm yr^{-1}, the vertical velocity of surface uplift induced by slab breakoff reaches up to ∼10 mm yr^{-1}, while it always remains below ∼4 mm yr^{-1} during the subsequent collision (Figure 3d). The horizontal migration of syn-collisional topographic uplift is also slower than the surface uplift propagation due to slab tearing (∼20 cm yr^{-1} and ∼75 cm yr^{-1} in reference model **1**; Figure 4g).

Similar to the slab tearing, differential collision becomes slower with increasing margin obliquity: for example, a change in obliquity angle from a reference value of 15° to 22.5° leads to a reduction in the rate of collision propagation from ∼20 cm yr^{-1} to ∼13 cm yr^{-1} (see Section 4.2). Furthermore, as expected, the decrease in the syn-collisional convergence velocity from a reference value of 4.5 cm yr^{-1} to 1.5 cm yr^{-1} also slows collision migration to a rate of ∼8 cm yr^{-1} (see Section 4.4), so that the velocity of plate convergence plays an important role in the dynamics of oblique collision and the associated history of topographic uplift (Figure 6g).

The presence of a microcontinent parallel to the original passive margin (Figure 10b-i) marks a more intense collision, as additional continental material is involved in the process (compare Figures 10a-iii and 10b-iii). The resulting along-strike variations in surface topography demonstrate a strong asymmetry (Figures 7 and 8) with a much more pronounced topographic growth in the segment of the convergent margin with microcontinent compared to the adjacent area without such additional complexities in the original structure of the passive margin (Figure 10b-iv).

5.2. Comparison of Modeling Results With Natural Examples

5.2.1. Natural Examples of Slab Tearing

Various geological observations, such as the lateral migration of the foreland basin depocenter, the along-strike propagation of mountain uplift, and the younging trend of magmatism, have been cited as surficial expressions of the horizontal propagation of slab breakoff (i.e., slab tearing; Ascione et al., 2012; Meulenkamp et al., 1996; Schlunegger & Kissling, 2022; van der Meulen et al., 1998). In the following, we discuss some tectonic settings for which slab tearing is proposed and compare them with the results of our numerical calculations (Figure 11).

In the Western/Central Alps, magmatic activity at ∼35–30 Ma has been interpreted as a consequence of the breakoff of the European slab (Davies & Von Blanckenburg, 1995; Handy et al., 2015; Schmid et al., 1996). Whether this slab breakoff continued horizontally below the Molasse Basin and, if so, how fast and in what way (horizontally, vertically or in combination) is still controversial (Eskens et al., 2024; Schlunegger & Kissling, 2022). Based on the lateral depocenter migration of foredeep basins along the Eastern Alps-Carpathians fold and thrust belt, it has been suggested that the tearing of the European slab occurred over a distance of ∼1,700 km, with the horizontal velocity accelerating from ∼7 to ∼45 cm yr^{-1} in the late Early to Middle Miocene (Meulenkamp et al., 1996). Our 3D numerical experiments show slab tearing velocities that are systematically higher, ranging from ∼38 to ∼118 cm yr^{-1} with most values >45 cm yr^{-1} (Figure 11a). It is important to note, however, that according to paleogeographic reconstructions, the Adria-Europe collision occurred along an irregular passive European margin (Handy et al., 2010; Le Breton et al., 2021). This irregularity was particularly pronounced in the Western and Central Alps due to the presence of the Briançonnais terrain (Manatschal & Müntener, 2009; Mohn et al., 2014). The implementation of such an extremely irregular passive margin by the highest initial obliquity (α = 22.5°; model **4**) or the inclusion of a microcontinent in combination with the reference obliquity (α = 15°; model **13**) leads to a reduction of the modeled tear propagation velocity, which in

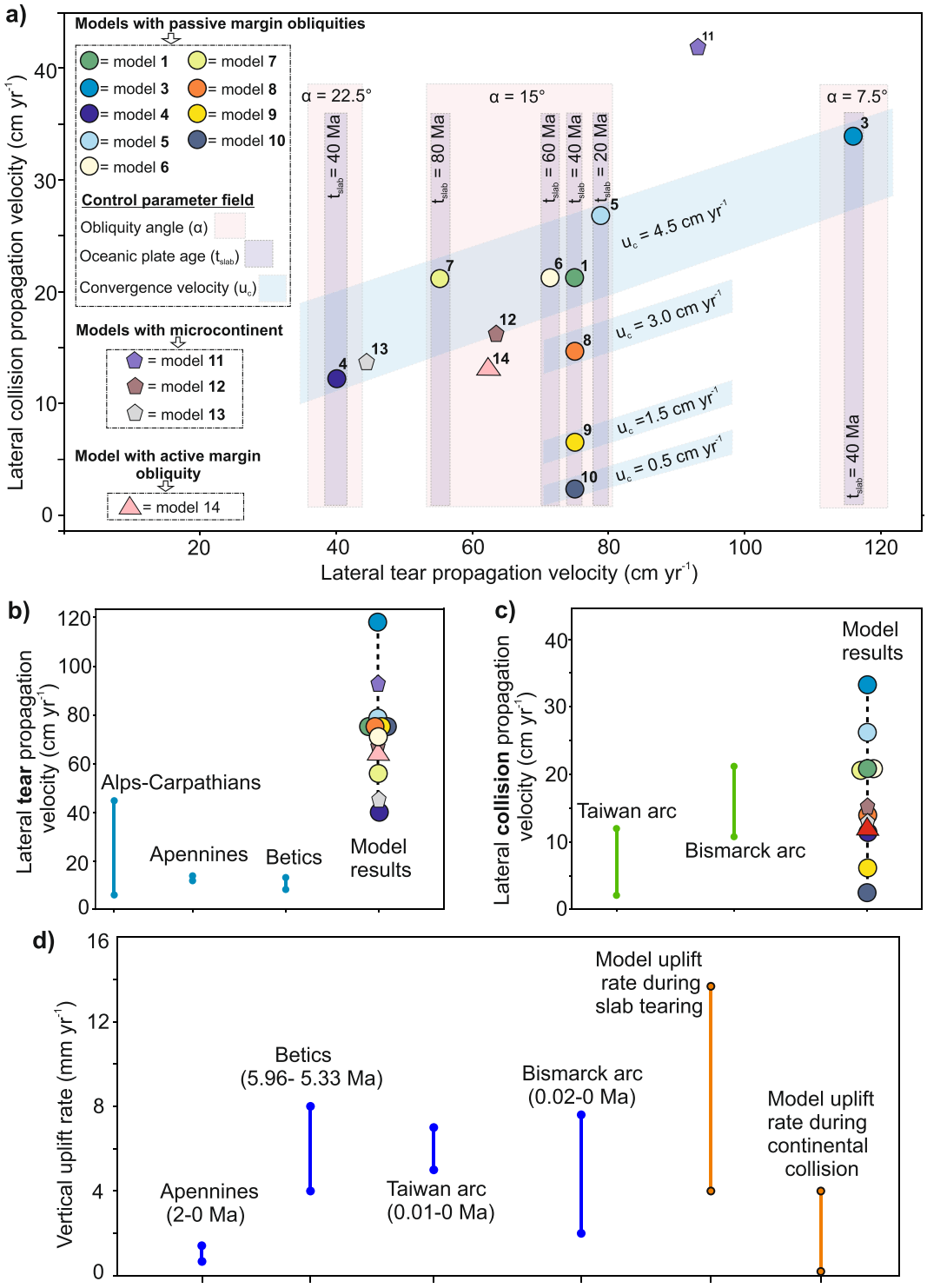

Figure 11.

these cases falls below 45 cm yr^{-1} (Figure 11a) and thus agrees better with the observations in the Alpine-Carpathian region (Figure 11b).

In the central and southern Apennines, stratigraphic analyses of Plio-Pleistocene wedge-top basins indicate a south-eastward migration of basin depocenter over a ∼140 km long distance, at an average rate of ∼12–14 cm yr^{-1} (Ascione et al., 2012). Such migration is interpreted as an expression of horizontal tear propagation within the Ionian slab. The tectonic configuration during the Ionian slab tearing corresponds to an originally oblique subduction trench retreating toward a non-oblique passive continental margin (Faccenna et al., 2001; Rosenbaum et al., 2008), which is similar to the configuration of model **14** (Figure 9). In agreement with the model results, the breakoff of the Ionian slab initiated at the northern Apennines and then propagated south-eastward from narrower to wider segments of the closing oceanic basin parallel to the original passive margin (Figures 9b–9d). Importantly, unlike other experiments where the initial passive margin was oblique, model **14** shows a non-pronounced gradient in topographic uplift along the orogen, which is also observed in the topography of the Apennines (Faccenna et al., 2014). The along-strike velocity of horizontal tear propagation in model **14** is however significantly higher (∼62 cm yr^{-1}; Figures 9c and 9d) than the estimates in the central and southern Apennines (∼12–14 cm yr^{-1}). A similar type of trench retreat leading to horizontal slab tear propagation is also proposed for the westernmost Mediterranean region beneath the Gibraltar Arc (Bezada et al., 2013; Lanari et al., 2023; Spakman et al., 2018), which has resulted in westward migration of intramountain basins uplift within the Betics and Rif (Boonma et al., 2023). Based on biostratigraphic proxies as a measure of marine uplift and westward uplift propagation (Garcés et al., 1998; Iribarren et al., 2009), the estimated velocity of tear propagation in this region ranges from ∼8 to ∼13.3 cm yr^{-1} (i.e., ∼400 km in ∼3–5 Myr), which is several times slower than in model **14** and all other presented experiments (Figures 11a and 11b).

The Aegean-Anatolian region has been proposed as a natural example of vertical slab tearing during the continental collision of Arabia with eastern Anatolia that began at ∼16 Ma. Concurrent with the collision, an adjacent western part of the Aegean slab retreated further to the south-west (Govers & Fichtner, 2016; Jolivet et al., 2013), thus resulting in the extension of the Aegean back-arc basin and the onset of vertical slab tearing beneath western Anatolia (Govers & Fichtner, 2016; Jolivet et al., 2013; Menant et al., 2016). Similar to previous modeling studies (e.g., Li et al., 2013; Menant et al., 2016), our models **12** and **13** successfully reproduce continental collision in the microcontinent area, which is separated from the simultaneous trench retreat of the adjacent slab segment by pronounced vertical tearing (Figure 8g and Figure S4g in Supporting Information S1). Interestingly, the experimentally estimated vertical tear propagation rate of ∼23 cm yr^{-1} is almost three times lower than the horizontal tearing velocity of ∼70 cm yr^{-1} (see Section 4.5).

To summarize, the velocities of slab tear propagation in all of the natural settings mentioned above are between ∼7 and ∼45 cm yr^{-1} (Figure 11b). This is in apparent contradiction to our modeling results (Figure 11a) and also to the findings of many other numerical studies, which predict that the velocity of slab tearing can be well above the estimated natural upper limit of ∼45 cm yr^{-1} and can reach up to ∼80–130 cm yr^{-1} (Andrić-Tomašević et al., 2023; Boonma et al., 2023; Burkett & Billen, 2010; van Hunen & Allen, 2011). Such a discrepancy between observations and modeling results may be caused by simplifications assumed in numerical experiments. For example, in all our 3D models as well as in most previous works, oceanic slabs are considered laterally homogeneous, which excludes any along-strike variation in their properties, including buoyancy and even strength. Given this assumption, it is not surprising that tearing in an absolutely homogeneous slab spreads extremely rapidly from one end to the other without any obstacle in the form of local stiffening along the way.

Figure 11. Slab tearing, collision propagation, and associated topographic uplift in models and in nature. (a) Lateral tear propagation versus lateral collision propagation velocities for models with different passive margin obliquities (model **1–10**), models with microcontinent (model **11–13**), and model with initial obliquity at the active margin side (model **14**). Note that different symbols with different colors are used to plot all the model results. Corresponding legends are shown on the left side of the panel (a). Additionally, for ready reference we have indicated the model number in the plot at the top-right corner of all the symbols. (b–d) Comparison between numerical model and natural examples for (b) lateral tear propagation velocity, (c) lateral collision propagation velocity, and (d) vertical uplift rate. Note that in panels (b and c) we use same symbol and color legends from panel (a) to plot the model results. In panel (c) we compare only oblique collision model results as both Taiwan and Bismarck arc represent oblique collisional settings (see Figure S8 in Supporting Information S1). All the natural observations data are taken from the following literature: Alps-Carpathians (Meulenkamp et al., 1996), Apennines (Ascione et al., 2012; Faccenna et al., 2014; van der Meulen et al., 1998), Betics (Garcés et al., 1998; Garcia-Castellanos & Villaseñor, 2011; Iribarren et al., 2009), Taiwan arc (Chen & Liu, 2000; Nagel et al., 2013), Bismarck arc in Papua New Guinea (Abbott et al., 1994; Crook, 1989; Silver et al., 1991).

However, it is well known that natural oceanic plates are not homogeneous and have inherent heterogeneities (e.g., Bendick & Ehlers, 2014; Nettesheim et al., 2018), such as varying thermal age, rheology, density, and geometric irregularities. Each of these factors may slow down the horizontal propagation of the slab tear and even cause the slab to be discontinuous and segmented, as often observed in nature (Chen et al., 2023). Additionally, irregularities in the structure of the passive continental margin (e.g., due to the presence of a microcontinent and/or a strong obliquity) can also reduce the slab tearing velocity, as demonstrated by our experiments (models **4** and **13**; Figure 11a). Finally, many of the observational studies mentioned above rely on the evolution of depositional environments in adjacent sedimentary basins to estimate the rate of tear propagation. It is noteworthy that the fingerprints of slab tearing retrieved from sedimentary basins should be used with caution and as indirect evidence, taking into account the time lag between the process of surface uplift, erosion, and final deposition of the sediments, which can range from several thousands to millions of years depending on other parameters such as basement erodibility, sea-level variations, gateways connections between marine domains, and climate (Cloetingh et al., 2023; Flowers & Ehlers, 2018; Herman et al., 2013; Schlunegger & Castelltort, 2016; Yanites et al., 2017).

5.2.2. Natural Examples of Along-Strike Differential Collision

In contrast to slab tearing rates, the velocities of orogenic uplift propagation observed in oblique collisional settings are consistent with our modeling estimates (Figure 11c), that range between ∼2 and ∼34 cm yr^{-1} (Figures 6g and 11a), depending on passive margin obliquities (α) and convergence velocities (u_c).

The first example is the Taiwan orogen, which formed by an oblique collision between the Luzon volcanic arc and the Asian passive margin (Barrier & Angelier, 1986; Chemenda et al., 2001). Paleoenvironmental and paleogeographical reconstructions constrain the southward propagation of orogenic uplift in the range of ∼2 cm yr^{-1} from ∼2 Ma to ∼0.5 Ma, and ∼10.6–12 cm yr^{-1} between ∼0.5 Ma and present (Nagel et al., 2013), although the initial rates (∼2 cm yr^{-1}) are not synchronous with the migration of the sediment depocenters (Nagel et al., 2013). Oblique collision in the Taiwan orogen occurred at an angle (α) of ∼30–33° (Chang et al., 2003; Figure S8a in Supporting Information S1) with a convergence velocity (u_c) of ∼7–8 cm yr^{-1}. Interestingly, even though these two parameters (α and u_c) are higher compared to the values tested in our study (Table 1), the resulting velocity of along-strike collision propagation (∼12 cm yr^{-1}) obtained in model **4** ($\alpha = 22.5°$, $u_c = 4.5$ cm yr^{-1}) is comparable to the upper estimates for the Taiwan orogen (∼10.6–12 cm yr^{-1}; Nagel et al., 2013). This similarity between the model predictions and the natural observations is likely due to the fact that the effects of the synchronous increase in α and u_c on collision propagation cancel each other out, given the revealed trends which indicate that as α and u_c increase, the collision rate decreases and increases, respectively (see sections 4.2 and 4.4).

Another example is Papua New Guinea, where oblique collision between the Bismarck arc and the Australian continental margin caused along-strike migration of orogenic uplift and associated changes of the depositional environment in the foreland basins (Galewsky & Silver, 1997). Collision in this region is known to have propagated in a south-eastward direction since 3.7–3.0 Ma (Abbott et al., 1994), whereas the modern collision tip is located in the western Solomon Sea (Galewsky & Silver, 1997). Based on plate geometry and convergence velocity, the rate of collision propagation is estimated to be ∼12–18 cm yr^{-1} (Silver et al., 1991), while an analysis of sedimentary facies in the foreland basin yielded a minimum value of ∼21.2 cm yr^{-1} (Silver et al., 1991) and ∼15.1 cm yr^{-1} (Abbott et al., 1994). According to paleotectonic reconstructions, the Bismarck arc collided with the Australian continental margin at an angle (α) of ∼30° with a convergence velocity (u_c) of ∼9.2–12.5 cm yr^{-1}. We hypothesize that a higher convergence rate (∼9.2–12.5 cm yr^{-1}) is the main reason for the lateral collision propagation, which is faster in the Bismarck arc collision region (∼21.2 cm yr^{-1}) than in the Taiwan orogen, where it only reaches ∼10.6–12 cm yr^{-1} at u_c of ∼7–8 cm yr^{-1} (Chang et al., 2003).

Interestingly, the observed velocities of along-strike uplift propagation due to both oblique collision and slab tearing fall in the strongly overlapping ranges of ∼2–22 cm yr^{-1} (Figure 11c) and ∼7–45 cm yr^{-1} (Figure 11b). In combination with the main outcome of our modeling that topographic uplift propagation induced by slab tearing is always much faster (∼38–118 cm yr^{-1}) than orogen migration related to oblique collision (∼2–34 cm yr^{-1}), this might suggest that the slowly migrating topographic uplift, commonly attributed to the process of slab tearing, could be related rather to oblique continental collision *sensu stricto*, thus justifying the need to reinterpret geodynamic scenarios for the evolution of some regions.

5.2.3. Vertical Uplift Rates

In addition to the horizontal velocities of orogenic front migration, the vertical rates of topographic uplift are another important output of our modeling, which can also be compared with natural observations for slab tearing and continental collision (Figure 11d). According to the modeling results, the topographic uplift rates during the continental collision phase are mainly controlled by the syn-collisional convergence velocities (Figures 6d–6f). For instance, at convergence velocities of 4.5, 3, and 1.5 cm yr^{-1}, the maximum topographic uplift rates are ∼4, ∼2.5, and ∼1.2 mm yr^{-1}, respectively (Figures 3d, 6d, and 6e). A similar trend is also observed in natural collisional settings. In particular, uplift rates in the Taiwan arc fall between ∼5 and ∼7 mm yr^{-1} for convergence velocities of ∼7–8 cm yr^{-1} (Chen & Liu, 2000; Nagel et al., 2013), whereas in the Bismarck arc region, where the convergence velocity is ∼9.3 cm yr^{-1} (Silver et al., 1991; Taylor, 1997), the uplift rate is ∼2.0–7.6 mm yr^{-1} (Crook, 1989). In all performed experiments, the vertical magnitude of the surface uplift rate during preceding phase of slab tearing is higher, reaching maximum values of up to ∼14 mm yr^{-1} for a very short duration of ∼0.1–0.2 Myr in experiments with non-oblique ($\alpha = 0°$; model **2**) or slightly oblique ($\alpha = 7.5°$; model **3**) passive margins (Figures 4d and 4e). At the higher passive margin obliquities ($\alpha = 15°$ and 22.5°), the maximum of tear related uplift is more moderate (∼10 mm yr^{-1}), while the values averaged over the period of slab tearing are between ∼4 and ∼8 mm yr^{-1} (models **1** and **4**; Figures 3d and 4f). A similar surface response to slab breakoff is hypothesized in the Gibraltar Arc region, where estimated critical uplift rates of ∼4–8 mm yr^{-1} (Garcia-Castellanos & Villaseñor, 2011) are required for the closure of Atlantic-Mediterranean seaway during Messinian salinity crisis at ∼5.93–5.66 Ma (Sternai et al., 2017).

6. Conclusions

In a series of 3D numerical simulations, we have explored the relative role of slab tearing and oblique retreating collision in the evolution of surface topography. The parametric analysis shows that the velocity of slab tear propagation and the associated horizontal migration of mountain uplift depend on the obliquity of the passive margin and the age of the oceanic slab. Our results emphasize the importance of the transition from oceanic to continental subduction in triggering slab breakoff, which occurs earlier than the collision *sensu stricto* and migrates in the form of an extremely fast slab tearing (∼38–118 cm yr^{-1}) from one side of the passive margin to the other due to an initially oblique configuration. On the contrary, the along-strike migration of topographic growth due to subsequent continental collision is always much slower (∼2–34 cm yr^{-1}) and is mainly controlled by the velocity of syn-collisional convergence and obliquity angle. These modeling results indicate that observations in nature, such as the relatively slow migration of basin depocenters and sedimentary facies changes, which are often interpreted as a consequence of slab tear propagation, might also be attributed to oblique continental collision. Similar to the velocities of horizontal topographic migration, the vertical uplift rates during slab tearing are much higher (maximum values of up to >10 mm yr^{-1}) than during the following collision phase (<4 mm yr^{-1}). Although the paleo-altimetry data and the reconstructed topographic uplift rates are subject to uncertainties, the modeled uplift rates, averaged over the period of slab tearing, generally correspond to the required critical values of ∼4–8 mm yr^{-1} in the Gibraltar Arc region during the Messinian salinity crisis. Finally, we demonstrate that a microcontinental block near the passive margin can bring additional complications, including more intense syn-collisional mountain building in the corresponding segment of the convergence zone. Furthermore, vertical slab tearing in the direction perpendicular to the trench may occur along the shorter edge of the microcontinent.

Data Availability Statement

The full version of the 3D thermomechanical code I3ELVIS with all input (in .t3c format) and output data (in .vtr and .grd formats) used to perform the experiments and generate the images presented in this study is freely available at Maiti et al. (2024). The open-source software Paraview version 5.11.1 (Ahrens et al., 2005), available under BSD 3-Clause license at https://www.paraview.org/resources/, is used to load and visualize the output data. Paraview States (in .pvsm format) for processing modeling results from .vtr files and the MATLAB script for visualizing the modeled topography from .grd files can also be found at Maiti et al. (2024).

Acknowledgments
This study was supported by the Deutsche Forschungsgemeinschaft (DFG) Grant to Nevena Andrić-Tomašević (TO 1364/1-1) within the priority program 4D-MB and contributed to the AlpArray initiative. Giridas Maiti thanks the Karlsruhe House of Young Scientists (KHYS) of Karlsruhe Institute of Technology for awarding connecting-young scientist travel grant, which enabled him to visit external collaborators while conducting this research. The authors gratefully acknowledge the support of the state of Baden-Württemberg through bwUniCluster (2.0). Taras Gerya acknowledge support by SNF Research Grant 200021_192296 and by ILP Task Force "Bio-geodynamics of the Lithosphere." All 3D numerical models were run in bwUniCluster (2.0) HPC, and access was provided by the Karlsruhe Institute of Technology. The manuscript benefitted from discussions with Marcel Thielmann, Andrea Piccolo, and Lucas Eskens. We thank two anonymous reviewers for their insightful and constructive suggestions and Editor Anke Friedrich for providing us a guideline to improve the manuscript. Open Access funding enabled and organized by Projekt DEAL.

References

Abbott, L. D., Silver, E. A., Thompson, P. R., Filewicz, M. V., & Schneider, C. (1994). Stratigraphic constraints on the development and timing of arc-continent collision in northern Papua New Guinea. *Journal of Sedimentary Research*, *B64*(2), 169–183. Retrieved from http://pubs.geoscienceworld.org/sepm/jsedres/article-pdf/64/2b/169/2811345/169.pdf

Ahrens, J., Geveci, B., & Law, C. (2005). ParaView: An end-user tool for large data visualization. In *Visualization handbook*. Elesvier. Retrieved from https://datascience.dsscale.org/wp-content/uploads/2016/06/ParaView.pdf

Andrić, N., Vogt, K., Matenco, L., Cvetković, V., Cloetingh, S., & Gerya, T. (2018). Variability of orogenic magmatism during Mediterranean-style continental collisions: A numerical modelling approach. *Gondwana Research*, *56*, 119–134. https://doi.org/10.1016/j.gr.2017.12.007

Andrić-Tomašević, N., Koptev, A., Maiti, G., Gerya, T., & Ehlers, T. A. (2023). Slab tearing in non-collisional settings: Insights from thermo-mechanical modelling of oblique subduction. *Earth and Planetary Science Letters*, *610*, 118097. https://doi.org/10.1016/j.epsl.2023.118097

Angrand, P., Ford, M., & Watts, A. B. (2018). Lateral variations in foreland flexure of a rifted continental margin: The Aquitaine Basin (SW France). *Tectonics*, *37*(2), 430–449. https://doi.org/10.1002/2017TC004670

Artemieva, I. M. (2006). Global 1° × 1° thermal model TC1 for the continental lithosphere: Implications for lithosphere secular evolution. *Tectonophysics*, *416*(1–2), 245–277. https://doi.org/10.1016/j.tecto.2005.11.022

Artyushkov, E. V. (1973). Stresses in the lithosphere caused by crustal thickness inhomogeneities. *Journal of Geophysical Research*, *78*(32), 7675–7708. https://doi.org/10.1029/jb078i032p07675

Ascione, A., Ciarcia, S., Di Donato, V., Mazzoli, S., & Vitale, S. (2012). The Pliocene-Quaternary wedge-top basins of southern Italy: An expression of propagating lateral slab tear beneath the Apennines. *Basin Research*, *24*(4), 456–474. https://doi.org/10.1111/j.1365-2117.2011.00534.x

Baitsch-Ghirardello, B., Gerya, T. V., & Burg, J. P. (2014). Geodynamic regimes of intra-oceanic subduction: Implications for arc extension vs. shortening processes. *Gondwana Research*, *25*(2), 546–560. https://doi.org/10.1016/j.gr.2012.11.003

Balázs, A., Faccenna, C., Ueda, K., Funiciello, F., Boutoux, A., Blanc, E. J. P., & Gerya, T. (2021). Oblique subduction and mantle flow control on upper plate deformation: 3D geodynamic modeling. *Earth and Planetary Science Letters*, *569*, 117056. https://doi.org/10.1016/j.epsl.2021.117056

Barrier, E., & Angelier, J. (1986). Active collision in eastern Taiwan: The coastal. *Tectonophysics*, *125*(1–3), 39–72. https://doi.org/10.1016/0040-1951(86)90006-5

Bendick, R., & Ehlers, T. A. (2014). Extreme localized exhumation at syntaxes initiated by subduction geometry. *Geophysical Research Letters*, *41*(16), 5861–5867. https://doi.org/10.1002/2014gl061026

Bercovici, D., & Ricard, Y. (2012). Mechanisms for the generation of plate tectonics by two-phase grain-damage and pinning. *Physics of the Earth and Planetary Interiors*, *202–203*, 27–55. https://doi.org/10.1016/j.pepi.2012.05.003

Bezada, M. J., Humphreys, E. D., Toomey, D. R., Harnafi, M., Dávila, J. M., & Gallart, J. (2013). Evidence for slab rollback in westernmost Mediterranean from improved upper mantle imaging. *Earth and Planetary Science Letters*, *368*, 51–60. https://doi.org/10.1016/j.epsl.2013.02.024

Bird, P., Liu, Z., & Rucker, W. K. (2008). Stresses that drive the plates from below: Definitions, computational path, model optimization, and error analysis. *Journal of Geophysical Research*, *113*(11), B11406. https://doi.org/10.1029/2007JB005460

Bittner, D., & Schmeling, H. (1995). Numerical modelling of melting processes and induced diapirism in the lower crust. *Geophysical Journal International*, *123*(1), 59–70. https://doi.org/10.1111/j.1365-246x.1995.tb06661.x

Boonma, K., García-Castellanos, D., Jiménez-Munt, I., & Gerya, T. (2023). Thermomechanical modelling of lithospheric slab tearing and its topographic response. *Frontiers in Earth Science*, *11*, 1095229. https://doi.org/10.3389/feart.2023.1095229

Boutoux, A., Briaud, A., Faccenna, C., Ballato, P., Rossetti, F., & Blanc, E. (2021). Slab folding and surface deformation of the Iran mobile belt. *Tectonics*, *40*(6), e2020TC006300. https://doi.org/10.1029/2020TC006300

Burkett, E. R., & Billen, M. I. (2010). Three-dimensionality of slab detachment due to ridge-trench collision: Laterally simultaneous boudinage versus tear propagation. *Geochemistry, Geophysics, Geosystems*, *11*(11), Q11012. https://doi.org/10.1029/2010GC003286

Burov, E. B. (2011). Rheology and strength of the lithosphere. *Marine and Petroleum Geology*, *28*(8), 1402–1443. https://doi.org/10.1016/j.marpetgeo.2011.05.008

Chang, C.-P., Angeiler, J., Lee, T.-Q., & Huang, C.-Y. (2003). From continental margin extension to collision orogen: Structural development and tectonic rotation of the Hengchun peninsula, southern Taiwan. *Tectonophysics*, *361*(1–2), 61–82. https://doi.org/10.1016/s0040-1951(02)00561-9

Chemenda, A. I., Yang, R.-K., Stephan, J.-F., Konstantinovskaya, E. A., & Ivanov, G. M. (2001). New results from physical modelling of arc±continent collision in Taiwan: Evolutionary model. Retrieved from www.elsevier.com/locate/tecto

Chen, Y., Chen, H., Liu, M., & Gerya, T. (2023). Vertical tearing of subducting plates controlled by geometry and rheology of oceanic plates. *Nature Communications*, *14*(1), 7931. https://doi.org/10.1038/s41467-023-43804-z

Chen, Y.-G., & Liu, T.-K. (2000). Holocene uplift and subsidence along an active tectonic margin southwestern Taiwan. *Quaternary Science Reviews*, *19*(9), 923–930. https://doi.org/10.1016/s0277-3791(99)00076-1

Clauser, C., & Huenges, E. (1995). Thermal conductivity of rocks and minerals. In T. Ahrens (Ed.), *Rock physics and phase relations. A handbook of physical constants* (pp. 105–126). American Geophysical Union. AGU Reference Shelf 3.

Cloetingh, S., Sternai, P., Koptev, A., Ehlers, T. A., Gerya, T., Kovács, I., et al. (2023). Coupled surface to deep Earth processes: Perspectives from TOPO-EUROPE with an emphasis on climate-and energy-related societal challenges. *Global and Planetary Change*, *226*, 104140. https://doi.org/10.1016/j.gloplacha.2023.104140

Connolly, J. A. D. (2005). Computation of phase equilibria by linear programming: A tool for geodynamic modeling and its application to subduction zone decarbonation. *Earth and Planetary Science Letters*, *236*(1–2), 524–541. https://doi.org/10.1016/j.epsl.2005.04.033

Crameri, F., Schmeling, H., Golabek, G. J., Duretz, T., Orendt, R., Buiter, S. J. H., et al. (2012). A comparison of numerical surface topography calculations in geodynamic modelling: An evaluation of the "sticky air" method. *Geophysical Journal International*, *189*(1), 38–54. https://doi.org/10.1111/j.1365-246X.2012.05388.x

Crook, K. A. W. (1989). Quaternary uplift rates at a plate boundary, Lae urban area, Papua New Guinea. *Tectonophysics*, *163*(1–2), 105–118. https://doi.org/10.1016/0040-1951(89)90121-2

Dai, L.-Q., Zhao, K., Zhao, Z.-F., Sun, G.-C., Gong, B., & Ma, L.-T. (2024). Slab subduction and pull link magmatism at active and passive continental margins. *Geophysical Research Letters*, *51*(1), e2023GL106218. https://doi.org/10.1029/2023GL106218

Darin, M. H., & Umhoefer, P. J. (2022). Diachronous initiation of Arabia–Eurasia collision from eastern Anatolia to the southeastern Zagros Mountains since middle Eocene time. *International Geology Review*, *64*(18), 2653–2681. https://doi.org/10.1080/00206814.2022.2048272

Davies, J. H., & Von Blanckenburg, F. (1995). Slab breakoff: A model of lithosphere detachment and its test in the magmatism and deformation of collisional orogens. *Earth and Planetary Science Letters*, *129*(1–4), 85–102. https://doi.org/10.1016/0012-821x(94)00237-s

Duretz, T., Gerya, T. V., & May, D. A. (2011). Numerical modelling of spontaneous slab breakoff and subsequent topographic response. *Tectonophysics*, *502*(1–2), 244–256. https://doi.org/10.1016/j.tecto.2010.05.024

Duretz, T., Gerya, T. V., & Spakman, W. (2014). Slab detachment in laterally varying subduction zones: 3-D numerical modeling. *Geophysical Research Letters*, *41*(6), 1951–1956. https://doi.org/10.1002/2014GL059472

England, P., & Molnar, P. (1990). Surface uplift, uplift of rocks, and exhumation of rocks. *Geology*, *18*(12), 1173–1177. https://doi.org/10.1130/0091-7613(1990)018<1173:suuora>2.3.co;2

Eskens, L. H. J., Andrić-Tomašević, N., Süss, P. M., Müller, M., Herrmann, R., & Ehlers, T. A. (2024). Lithospheric- and crustal scale controls on variations in foreland basin development in the Northern Alpine Foreland Basin. *Tectonophysics*, *878*, 230283. https://doi.org/10.1016/j.tecto.2024.230283

Faccenna, C., Becker, T. W., Lucente, F. P., Jolivet, L., & Rossetti, F. (2001). History of subduction and back-arc extension in the Central Mediterranean. *Geophysical Journal International*, *145*(3), 809–820. https://doi.org/10.1046/j.0956-540x.2001.01435.x

Faccenna, C., Becker, T. W., Miller, M. S., Serpelloni, E., & Willett, S. D. (2014). Isostasy, dynamic topography, and the elevation of the Apennines of Italy. *Earth and Planetary Science Letters*, *407*, 163–174. https://doi.org/10.1016/j.epsl.2014.09.027

Flowers, R. M., & Ehlers, T. A. (2018). Rock erodibility and the interpretation of low-temperature thermochronologic data. *Earth and Planetary Science Letters*, *482*, 312–323. https://doi.org/10.1016/j.epsl.2017.11.018

Galewsky, J., & Silver, E. A. (1997). Tectonic controls on facies transitions in an oblique collision: The western Solomon Sea, Papua New Guinea. *GSA Bulletin*, *109*(10), 1266–1278. https://doi.org/10.1130/0016-7606(1997)109<1266:tcofti>2.3.co;2

Garcés, M., Krijgsman, W., & Agustí, J. (1998). Chronology of the late Turolian deposits of the Fortuna basin (SE Spain): Implications for the Messinian evolution of the eastern Betics. *Earth and Planetary Science Letters*, *163*(1–4), 69–81. https://doi.org/10.1016/s0012-821x(98)00176-9

Garcia-Castellanos, D., & Villaseñor, A. (2011). Messinian salinity crisis regulated by competing tectonics and erosion at the Gibraltar arc. *Nature*, *480*(7377), 359–363. https://doi.org/10.1038/nature10651

Garzanti, E., Radeff, G., & Malusà, M. G. (2018). Slab breakoff: A critical appraisal of a geological theory as applied in space and time. *Earth-Science Reviews*, *177*, 303–319. https://doi.org/10.1016/j.earscirev.2017.11.012

Gerya, T. (2019). *Introduction to numerical geodynamic modelling* (2nd ed., p. 471). Cambridge University Press.

Gerya, T. V., Bercovici, D., & Becker, T. W. (2021). Dynamic slab segmentation due to brittle–ductile damage in the outer rise. *Nature*, *599*(7884), 245–250. https://doi.org/10.1038/s41586-021-03937-x

Gerya, T. V., & Meilick, F. I. (2011). Geodynamic regimes of subduction under an active margin: Effects of rheological weakening by fluids and melts. *Journal of Metamorphic Geology*, *29*(1), 7–31. https://doi.org/10.1111/j.1525-1314.2010.00904.x

Gerya, T. V., Perchuk, L. L., & Burg, J. P. (2008). Transient hot channels: Perpetrating and regurgitating ultrahigh-pressure, high-temperature crust-mantle associations in collision belts. *Lithos*, *103*(1–2), 236–256. https://doi.org/10.1016/j.lithos.2007.09.017

Gerya, T. V., Stern, R. J., Baes, M., Sobolev, S. V., & Whattam, S. A. (2015). Plate tectonics on the Earth triggered by plume-induced subduction initiation. *Nature*, *527*(7577), 221–225. https://doi.org/10.1038/nature15752

Gerya, T. V., & Yuen, D. A. (2003). Characteristics-based marker-in-cell method with conservative finite-differences schemes for modeling geological flows with strongly variable transport properties. *Physics of the Earth and Planetary Interiors*, *140*(4), 293–318. https://doi.org/10.1016/j.pepi.2003.09.006

Gerya, T. V., & Yuen, D. A. (2007). Robust characteristics method for modelling multiphase visco-elasto-plastic thermo-mechanical problems. *Physics of the Earth and Planetary Interiors*, *163*(1–4), 83–105. https://doi.org/10.1016/j.pepi.2007.04.015

Gerya, T. V., Yuen, D. A., & Maresch, W. V. (2004). Thermomechanical modelling of slab detachment. *Earth and Planetary Science Letters*, *226*(1–2), 101–116. https://doi.org/10.1016/j.epsl.2004.07.022

Göğüş, O. H., & Pysklywec, R. N. (2008). Near-surface diagnostics of dripping or delaminating lithosphere. *Journal of Geophysical Research*, *113*, B11404. https://doi.org/10.1029/2007jb005123

Govers, R., & Fichtner, A. (2016). Signature of slab fragmentation beneath Anatolia from full-waveform tomography. *Earth and Planetary Science Letters*, *450*, 10–19. https://doi.org/10.1016/j.epsl.2016.06.014

Gül, M., Gürbüz, K., & Cronin, B. T. (2015). Irregular plate boundary controls on Foreland Basin sedimentation (Miocene, Kahramanmaraş Foreland Basin, SE Turkey). *Journal of Asian Earth Sciences*, *111*, 804–818. https://doi.org/10.1016/j.jseaes.2015.07.018

Gün, E., Pysklywec, R. N., Göğüş, O. H., & Topuz, G. (2021). Pre-collisional extension of microcontinental terranes by a subduction pulley. *Nature Geoscience*, *14*(6), 443–450. https://doi.org/10.1038/s41561-021-00746-9

Handy, M. R., M. Schmid, S., Bousquet, R., Kissling, E., & Bernoulli, D. (2010). Reconciling plate-tectonic reconstructions of Alpine Tethys with the geological-geophysical record of spreading and subduction in the Alps. *Earth-Science Reviews*, *102*(3–4), 121–158. https://doi.org/10.1016/j.earscirev.2010.06.002

Handy, M. R., Ustaszewski, K., & Kissling, E. (2015). Reconstructing the Alps–Carpathians–Dinarides as a key to understanding switches in subduction polarity, slab gaps and surface motion. *International Journal of Earth Sciences*, *104*(1), 1–26. https://doi.org/10.1007/s00531-014-1060-3

Herman, F., Seward, D., Valla, P. G., Carter, A., Kohn, B., Willett, S. D., & Ehlers, T. A. (2013). Worldwide acceleration of mountain erosion under a cooling climate. *Nature*, *504*(7480), 423–426. https://doi.org/10.1038/nature12877

Hirth, G., & Kohlstedt, D. (2004). Rheology of the upper mantle and the mantle wedge: A view from the experimentalists. In *Geophysical monograph series* (Vol. 138, pp. 83–105). Blackwell Publishing Ltd. https://doi.org/10.1029/138GM06

Huang, Z., Wang, L., Zhao, D., Xu, M., Mi, N., Yu, D., et al. (2010). Upper mantle structure and dynamics beneath Southeast China. *Physics of the Earth and Planetary Interiors*, *182*(3–4), 161–169. https://doi.org/10.1016/j.pepi.2010.07.010

Huismans, R. S., & Beaumont, C. (2003). Symmetric and asymmetric lithospheric extension: Relative effects of frictional-plastic and viscous strain softening. *Journal of Geophysical Research*, *108*(B10), 2496. https://doi.org/10.1029/2002JB002026

Iribarren, L., Vergés, J., & Fernàndez, M. (2009). Sediment supply from the Betic-Rif orogen to basins through Neogene. *Tectonophysics*, *475*(1), 68–84. https://doi.org/10.1016/j.tecto.2008.11.029

Jolivet, L., Faccenna, C., Huet, B., Labrousse, L., Le Pourhiet, L., Lacombe, O., et al. (2013). Aegean tectonics: Strain localisation, slab tearing and trench retreat. *Tectonophysics*, *597–598*, 1–33. https://doi.org/10.1016/j.tecto.2012.06.011

Koptev, A., Beniest, A., Gerya, T., Ehlers, T. A., Jolivet, L., & Leroy, S. (2019). Plume-induced breakup of a subducting plate: Microcontinent formation without cessation of the subduction process. *Geophysical Research Letters*, *46*(7), 3663–3675. https://doi.org/10.1029/2018GL081295

Koptev, A., Cloetingh, S., Gerya, T., Sternai, P., & Botsyun, S. (2022). Ocean-continent subduction cannot be initiated without preceding intra-oceanic subduction!. *Frontiers in Earth Science*, *10*, 1097922. https://doi.org/10.3389/feart.2022.1097922

Koptev, A., Cloetingh, S., Kovács, I. J., Gerya, T., & Ehlers, T. A. (2021). Controls by rheological structure of the lithosphere on the temporal evolution of continental magmatism: Inferences from the Pannonian Basin system. *Earth and Planetary Science Letters*, *565*, 116925. https://doi.org/10.1016/j.epsl.2021.116925

Koptev, A. I., & Ershov, A. V. (2010). The role of the gravitational potential of the lithosphere in the formation of a global stress field. *Izvestiya - Physics of the Solid Earth*, *46*(12), 1080–1094. https://doi.org/10.1134/S1069351310120050

Koptev, A. I., & Ershov, A. V. (2011). Thermal thickness of the Earth's lithosphere: A numerical model. *Moscow University Geology Bulletin*, *66*(5), 323–330. https://doi.org/10.3103/s014587521105005x

Kuhlemann, J., & Kempf, O. (2002). Post-Eocene evolution of the North Alpine Foreland Basin and its response to Alpine tectonics. *Sedimentary Geology*, *152*(1–2), 45–78. https://doi.org/10.1016/s0037-0738(01)00285-8

Lallemand, S., Heuret, A., Faccenna, C., & Funiciello, F. (2008). Subduction dynamics as revealed by trench migration. *Tectonics*, *27*(3), TC3014. https://doi.org/10.1029/2007TC002212

Lanari, R., Boutoux, A., Faccenna, C., Herman, F., Willett, S. D., & Ballato, P. (2023). Cenozoic exhumation in the Mediterranean and the Middle East. *Earth-Science Reviews*, *237*, 104328. https://doi.org/10.1016/j.earscirev.2023.104328

Lash, G. G. (1998). Along-strike variations in foreland basin evolution: Possible evidence for continental collision along an irregular margin. *Basin Research*, *1*(2), 71–83. https://doi.org/10.1111/j.1365-2117.1988.tb00006.x

Le Breton, E., Brune, S., Ustaszewski, K., Zahirovic, S., Seton, M., & Müller, R. D. (2021). Kinematics and extent of the Piemont-Liguria Basin-implications for subduction processes in the Alps. *Solid Earth*, *12*(4), 885–913. https://doi.org/10.5194/se-12-885-2021

Li, Y., & Gurnis, M. (2023). A simple force balance model of subduction initiation. *Geophysical Journal International*, *232*(1), 128–146. https://doi.org/10.1093/gji/ggac332

Li, Z. H., Xu, Z., Gerya, T., & Burg, J. P. (2013). Collision of continental corner from 3-D numerical modeling. *Earth and Planetary Science Letters*, *380*, 98–111. https://doi.org/10.1016/j.epsl.2013.08.034

Magni, V., Faccenna, C., van Hunen, J., & Funiciello, F. (2013). Delamination vs. break-off: The fate of continental collision. *Geophysical Research Letters*, *40*(2), 285–289. https://doi.org/10.1002/grl.50090

Maiti, G., Koptev, A., Baville, P., Gerya, T., Crosetto, S., & Andrić-Tomašević, N. (2024). Topography response to horizontal slab tearing and oblique continental collision: 3D thermomechanical numerical modelling [Dataset]. *Zenodo*. https://doi.org/10.5281/zenodo.13759429

Maiti, G., Roy, A., Sen, J., & Mandal, N. (2021). Impact of decelerating India-Asia convergence on the crustal flow kinematics in Tibet: An insight from scaled laboratory modeling. *Geochemistry, Geophysics, Geosystems*, *22*(11), e2021GC009967. https://doi.org/10.1029/2021GC009967

Malatesta, C., Gerya, T., Crispini, L., Federico, L., & Capponi, G. (2016). Interplate deformation at early-stage oblique subduction: 3-D thermomechanical numerical modeling. *Tectonics*, *35*(7), 1610–1625. https://doi.org/10.1002/2016TC004139

Manatschal, G., & Müntener, O. (2009). A type sequence across an ancient magma-poor ocean-continent transition: The example of the western Alpine Tethys ophiolites. *Tectonophysics*, *473*(1–2), 4–19. https://doi.org/10.1016/j.tecto.2008.07.021

Menant, A., Sternai, P., Jolivet, L., Guillou-Frottier, L., & Gerya, T. (2016). 3D numerical modeling of mantle flow, crustal dynamics and magma genesis associated with slab roll-back and tearing: The eastern Mediterranean case. *Earth and Planetary Science Letters*, *442*, 93–107. https://doi.org/10.1016/j.epsl.2016.03.002

Meulenkamp, J. E., Kováč, M., & Cicha, I. (1996). On Late Oligocene to Pliocene depocentre migrations and the evolution of the Carpathian-Pannonian system. *Tectonophysics*, *266*(1–4), 301–317. https://doi.org/10.1016/s0040-1951(96)00195-3

Mohn, G., Manatschal, G., Beltrando, M., & Haupert, I. (2014). The role of rift-inherited hyper-extension in Alpine-type orogens. *Terra Nova*, *26*(5), 347–353. https://doi.org/10.1111/ter.12104

Müller, R. D., Gaina, C., Roest, W. R., & Hansen, D. L. (2001). A recipe for microcontinent formation. *Geology*, *29*(3), 203. https://doi.org/10.1130/0091-7613(2001)029<0203:arfmf>2.0.co;2

Mulyukova, E., & Bercovici, D. (2017). Formation of lithospheric shear zones: Effect of temperature on two-phase grain damage. *Physics of the Earth and Planetary Interiors*, *270*, 195–212. https://doi.org/10.1016/j.pepi.2017.07.011

Munch, J., Ueda, K., Schnydrig, S., May, D. A., & Gerya, T. V. (2022). Contrasting influence of sediments vs surface processes on retreating subduction zones dynamics. *Tectonophysics*, *836*, 229410. https://doi.org/10.1016/j.tecto.2022.229410

Nagel, S., Castelltort, S., Wetzel, A., Willett, S. D., Mouthereau, F., & Lin, A. T. (2013). Sedimentology and foreland basin paleogeography during Taiwan arc continent collision. *Journal of Asian Earth Sciences*, *62*, 180–204. https://doi.org/10.1016/j.jseaes.2012.09.001

Nettesheim, M., Ehlers, T. A., Whipp, D. M., & Koptev, A. (2018). The influence of upper-plate advance and erosion on overriding plate deformation in orogen syntaxes. *Solid Earth*, *9*(6), 1207–1224. https://doi.org/10.5194/se-9-1207-2018

O'Brien, P. J. (2001). Subduction followed by collision: Alpine and Himalayan examples. *Physics of the Earth and Planetary Interiors*, *127*(1–4), 277–291. https://doi.org/10.1016/s0031-9201(01)00232-1

Putirka, K. D., Perfit, M., Ryerson, F. J., & Jackson, M. G. (2007). Ambient and excess mantle temperatures, olivine thermometry, and active vs. passive upwelling. *Chemical Geology*, *241*(3–4), 177–206. https://doi.org/10.1016/j.chemgeo.2007.01.014

Pysklywec, R. N., Beaumont, C., & Fullsack, P. (2000). Modeling the behavior of the continental mantle lithosphere during plate convergence. *Geology*, *28*(7), 655–658. https://doi.org/10.1130/0091-7613(2000)028<0655:mtbotc>2.3.co;2

Ranalli, G. (1995). *Rheology of the Earth*. (p. 413). Chapman & Hall.

Rosenbaum, G., Gasparon, M., Lucente, F. P., Peccerillo, A., & Miller, M. S. (2008). Kinematics of slab tear faults during subduction segmentation and implications for Italian magmatism. *Tectonics*, *27*(2), TC2008. https://doi.org/10.1029/2007TC002143

Schlunegger, F., & Castelltort, S. (2016). Immediate and delayed signal of slab breakoff in Oligo/Miocene Molasse deposits from the European Alps. *Scientific Reports*, *6*(1), 31010. https://doi.org/10.1038/srep31010

Schlunegger, F., & Kissling, E. (2022). Slab load controls beneath the Alps on the source-to-sink sedimentary pathways in the Molasse Basin. *Geosciences*, *12*(6), 226. https://doi.org/10.3390/geosciences12060226

Schmeling, H., Babeyko, A. Y., Enns, A., Faccenna, C., Funiciello, F., Gerya, T., et al. (2008). A benchmark comparison of spontaneous subduction models-Towards a free surface. *Physics of the Earth and Planetary Interiors*, *171*(1–4), 198–223. https://doi.org/10.1016/j.pepi.2008.06.028

Schmid, S. M., Pfiffner, O. A., Froitzheim, N., Schönborn, G., & Kissling, E. (1996). Geophysical-geological transect and tectonic evolution of the Swiss-Italian Alps. *Tectonics*, *15*(5), 1036–1064. https://doi.org/10.1029/96TC00433

Silver, E. A., Abbott, L. D., Kirchoff-Stein, K. S., Reed, D. L., Bernstein-Taylor, B., & Hilyard, D. (1991). Collision propagation in Papua New Guinea and the Solomon sea. *Tectonics*, *10*(5), 863–874. https://doi.org/10.1029/91tc00867

Sinclair, H. D. (1997). Flysch to molasse transition in peripheral foreland basins: The role of the passive margin versus slab breakoff. *Geology*, *25*(12), 1123–1126. https://doi.org/10.1130/0091-7613(1997)025<1123:ftmtip>2.3.co;2

Sizova, E., Hauzenberger, C., Fritz, H., Faryad, S. W., & Gerya, T. (2019). Late orogenic heating of (ultra)high pressure rocks: Slab Rollback vs. Slab breakoff. *Geosciences*, *9*(12), 499. https://doi.org/10.3390/geosciences9120499

Sleep, N. H. (2003). Geodynamic implications of xenolith geotherms. *Geochemistry, Geophysics, Geosystems*, *4*(9), 1079. https://doi.org/10.1029/2003GC000511

Spakman, W., Chertova, M. V., Van Den Berg, A., & Van Hinsbergen, D. J. J. (2018). Puzzling features of western Mediterranean tectonics explained by slab dragging. *Nature Geoscience*, *11*(3), 211–216. https://doi.org/10.1038/s41561-018-0066-z

Stern, R. J., & Gerya, T. (2018). Subduction initiation in nature and models: A review. *Tectonophysics*, *746*, 173–198. https://doi.org/10.1016/j.tecto.2017.10.014

Sternai, P. (2020). Surface processes forcing on extensional rock melting. *Scientific Reports*, *10*(1), 7711. https://doi.org/10.1038/s41598-020-63920-w

Sternai, P., Caricchi, L., Garcia-Castellanos, D., Jolivet, L., Sheldrake, T. E., & Castelltort, S. (2017). Magmatic pulse driven by sea-level changes associated with the Messinian salinity crisis. *Nature Geoscience*, *10*(10), 783–787. https://doi.org/10.1038/ngeo3032

Sternai, P., Jolivet, L., Menant, A., & Gerya, T. (2014). Driving the upper plate surface deformation by slab rollback and mantle flow. *Earth and Planetary Science Letters*, *405*, 110–118. https://doi.org/10.1016/j.epsl.2014.08.023

Stockmal, G. S., Colman-Sadd, S. P., Keen, C. E., O'Brien, S. J., & Quinlan, G. (1987). Collision along an irregular margin: A regional plate tectonic interpretation of the Canadian Appalachians. *Journal of Earth Sciences*, *24*(6), 1098–1107. https://doi.org/10.1139/e87-107

Taylor, B. (1997). Bismarck sea-evolution of a back-arc basin. *Geology*, *7*(4), 171–174. https://doi.org/10.1130/0091-7613(1979)7<171:bseoab>2.0.co;2

Tesauro, M., Maierová, P., Koptev, A., Pastorutti, A., Pivetta, T., Koulakov, I., & Braitenberg, C. (2024). What controls structural variations along the Zagros Collision Zone? Insights from geophysical observations and thermo-mechanical modelling. *Gondwana Research*, *133*, 297–322. https://doi.org/10.1016/j.gr.2024.06.009

Turcotte, D. L., & Schubert, G. (2002). *Geodynamics*. (p. 863). Cambridge University Press.

Ueda, K., Willett, S. D., Gerya, T., & Ruh, J. (2015). Geomorphological–thermo-mechanical modeling: Application to orogenic wedge dynamics. *Tectonophysics*, *659*, 12–30. https://doi.org/10.1016/j.tecto.2015.08.001

van der Meulen, M. J., Meulenkamp, J. E., & Wortel, M. J. R. (1998). Lateral shifts of Apenninic foredeep depocentres reflecting detachment of subducted lithosphere. *Earth and Planetary Science Letters*, *154*(1–4), 203–219. https://doi.org/10.1016/s0012-821x(97)00166-0

van Hunen, J., & Allen, M. B. (2011). Continental collision and slab break-off: A comparison of 3-D numerical models with observations. *Earth and Planetary Science Letters*, *302*(1–2), 27–37. https://doi.org/10.1016/j.epsl.2010.11.035

Vergés, J., & Fernàndez, M. (2012). Tethys-Atlantic interaction along the Iberia-Africa plate boundary: The Betic-Rif orogenic system. *Tectonophysics*, *579*, 144–172. https://doi.org/10.1016/j.tecto.2012.08.032

Wortel, M., & Spakman, W. (1992). Structure and dynamics of subducted lithosphere in the Mediterranean region. In *Proceedings of the koninklijke nederlandse akademie van Wetenschappen/C* (Vol. 95, pp. 325–347).

Wortel, M., & Spakman, W. (2000). Subduction and slab detachment in the Mediterranean–Carpathian region. *Science*, *290*(5498), 1910–1917. https://doi.org/10.1126/science.290.5498.1910

Yanites, B. J., Becker, J. K., Madritsch, H., Schnellmann, M., & Ehlers, T. A. (2017). Lithologic effects on landscape response to base level changes: A modeling study in the context of the eastern Jura mountains, Switzerland. *Journal of Geophysical Research: Earth Surface*, *122*(11), 2196–2222. https://doi.org/10.1002/2016JF004101

Zhu, D. C., Wang, Q., Zhao, Z. D., Chung, S. L., Cawood, P. A., Niu, Y., et al. (2015). Magmatic record of India-Asia collision. *Scientific Reports*, *5*(1), 14289. https://doi.org/10.1038/srep14289